SLAC-PUB-14801

An invited review article for ***Frontiers of Physics in China***

High energy $\gamma-$ray emission from Gamma-Ray Bursts – before GLAST

Yi-Zhong Fan*
Niels Bohr International Academy, Niels Bohr Institute, Blegdamsvej 17, DK-2100 Copenhagen, Denmark
Purple Mountain Observatory, Chinese Academy of Sciences, Nanjing 210008, China

Tsvi Piran†
The Racah Inst. of Physics, Hebrew University, Jerusalem 91904, Israel
(Dated: May 6, 2009)

Gamma-ray bursts (GRBs) are short and intense emission of soft $\gamma-$rays, which have fascinated astronomers and astrophysicists since their unexpected discovery in 1960s. The X-ray/optical/radio afterglow observations confirm the cosmological origin of GRBs, support the fireball model, and imply a long-activity of the central engine. The high energy $\gamma-$ray emission (> 20 MeV) from GRBs is particularly important because they shed some lights on the radiation mechanisms and can help us to constrain the physical processes giving rise to the early afterglows. In this work, we review observational and theoretical studies of the high energy emission from GRBs. Special attention is given to the expected high energy emission signatures accompanying the canonical early-time X-ray afterglow that was observed by the Swift X-ray Telescope. We also discuss the detection prospect of the upcoming GLAST satellite and the current ground-based Cerenkov detectors.

PACS numbers: 95.30.Gv, 95.85.Pw, 98.70.Rz

I. INTRODUCTION

Gamma-ray bursts (GRBs) are brief intense flashes of soft ($0.01-1$ MeV) γ-rays that are detected once or twice a day for a BATSE-like detector. GRBs were serendipitously discovered by Vela satellites in late 1960s, and were first publicly reported by Klebesadel et al. in 1973 [1]. The observed bursts arrive from apparently random directions in the sky and they last between tens of millisecond and thousands of seconds [2]. Their physical origin has been debated for a long time mainly due to the lack of an exact position and a reliable estimate of the distance to us. In 1997, several GRBs were rapidly and accurately localized by the Italian-Dutch BeppoSAX satellite, leading to the discovery of their X-ray, optical and radio counterparts, and their redshifts [3, 4, 5, 6]. The cosmological origin of most, if not all GRBs, was confirmed. The leading interpretation of the data is the cosmological fireball model [7, 8, 9, 10, 11, 12, 13, 14, 15, 16], in which the prompt $\gamma-$rays are powered by the baryon-rich (or Poynting flux) relativistic jets ejected from the central engine with variable Lorentz factors (i.e., internal shocks) while the afterglows are produced by the interaction between the outflow material and the medium (i.e., external shocks).

The most widely discussed radiation mechanisms include synchrotron emission and inverse Compton (IC) scattering. Both can produce electromagnetic emission in a very wide energy range, i.e., radio to hard $\gamma-$rays (GeV or even TeV). Like in Active galactic nucleus (AGNs) we expect that the IC process will give rise to a high energy component that will be emitted along with the prompt sub-MeV photons and the afterglow radio/optical/X-ray emission, as detected in dozens of GRBs by the Compton Gamma Ray Observatory (CGRO) satellite in $1991-2000$ [17, 18, 19, 20, 21, 22, 23]. For example if the typical synchrotron frequency of the prompt emission is 100 keV and the electrons have a Lorentz factor of 500 (in internal shocks) we expect IC emission peaks at ~ 20 GeV. Similarly, inverse Compton of reverse shock photons with ~ 1 eV by forwards shock electrons with a Lorentz factor of 10^4 will result in an IC component of ~ 100 MeV.

The Large Area Telescope (LAT) onboard the Gamma Ray Large Area Space Telescope (GLAST; see http://glast.gsfc.nasa.gov/), to be launched soon, is expected to enhance high energy detection rate significantly because of its larger effective area than that of EGRET. For a bright burst at a redshift $z \sim 1$, LAT may collect ~ 10 tens-MeV to GeV afterglow photons [24]. The estimate of the detectability of the prompt high energy $\gamma-$rays is more difficult because the physical parameters involved in the internal shocks are still poorly constrained. Regardless of the uncertainties, preliminary calculations suggest a promising detection prospect for LAT [25, 26].

The high energy emission from GRBs can help us to better understand the physical composition of the outflow, the radiation mechanisms, and the underlying physical processes shaping the early afterglow. Such goals, of course, are hard to achieve because of the rarity of the high energy photons. However, with LAT, $\sim 10^3$ high energy photons could be detected from an extremely bright

Work supported in part by US Department of Energy contract DE-AC02-76SF00515.

SLAC National Accelerator Laboratory, Menlo Park, CA 94025

burst (for example, GRB 940217, GRB 030329 and GRB 080319B) and these can be used to constrain the models. With such a hope, we present in this work an overview of the theoretical studies of high energy emission from GRBs.

The structure of this review is as follows. We first discuss the observational aspects of high energy emission of GRBs and afterglows in Section II, and then the physical processes in Section III. We discuss the high energy emission processes in GRBs and afterglows, the interpretations of available high energy observations and possible progresses in the next decade in Sections IV-VI, respectively.

II. OBSERVATIONS

We begin with a short review of the observations of high energy emission from GRBs and afterglows. We divide this section into four parts, beginning with an introduction of the detectors. We then have a short discussion of the cosmic absorption of high energy $\gamma-$rays, that plays a crucial role in the detection prospects above 50 GeV. We continue with the prompt high energy emission– the GRB itself but in energies above 20MeV and properties of high energy afterglows.

A. Detectors

Space telescopes. Among space telescopes dedicated to high energy $\gamma-$ray astrophysics, three are particularly interesting for GRB people, including the Energetic Gamma Ray Experiment Telescope (EGRET) onboard CGRO (see http://heasarc.gsfc.nasa.gov/docs/cgro/egret/), Gamma-Ray Imaging Detector (GRID) onboard AGILE (see http://agile.rm.iasf.cnr.it/), and the upcoming LAT onboard GLAST satellite. EGRET and GRID have a similar peak effective area ~ 1000 cm^2. That of LAT, however, is much larger. We compare them in Table I. With a higher sensitivity, LAT is expect to detect high energy photons from GRBs much more frequently than both EGRET and GRID. The Burst Monitor (GBM) onboard GLAST is sensitive to X-rays and gamma rays with energies between 8 keV and 25 MeV. The combination of GBM and LAT provides a powerful tool for studying gamma-ray bursts, particularly for time-resolved spectral studies over a very broad energy band.

The effective area of the LAT as a function of photon energy is shown in the upper panel of Fig.1. For photons below 100 MeV, the effective area of LAT is small, which limits the detection prospect of the MeV photons. GBM won't help in this aspect because of its rather small area ~ 126 cm^2. The high energy photons are much less numerous than the keV-MeV photons because of the large energy each photon carries. So even in the most optimistic extreme cases, the number of high energy photons detected by GLAST-like satellites is not expected to be much more than $\sim 10^3$.

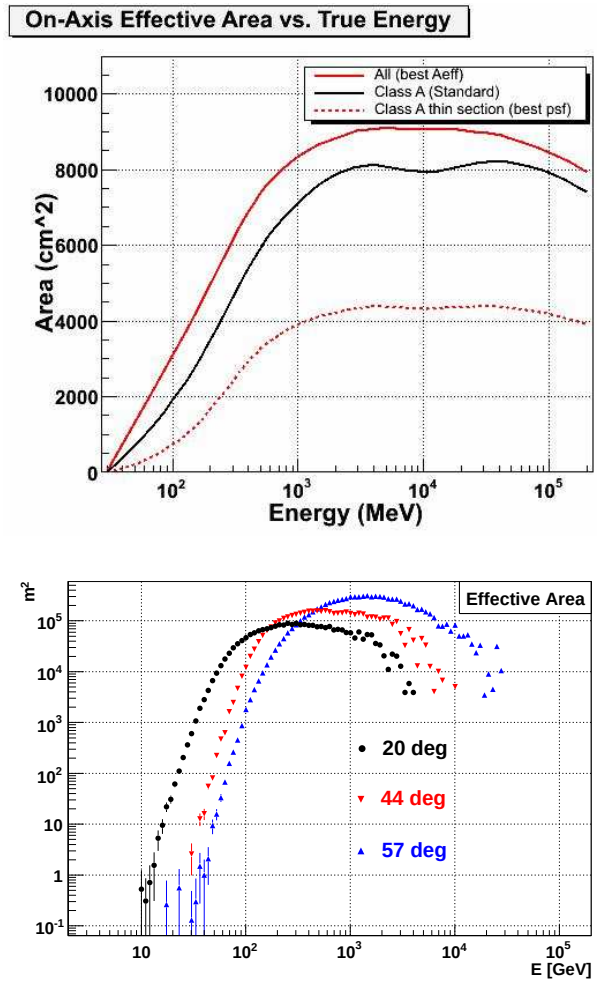

FIG. 1: Upper panel: On-axis effective areas of LAT (from http://www-glast.slac.stanford.edu/software/IS/glast_lat_performance.h Lower panel: Effective area of MAGIC for three different zenith angles (from [29]).

Ground-based telescopes. Ground-based high energy detectors have very large effective areas $\sim 10^4 - 10^5$ m^2 but work in the energy range of tens GeV to 100 TeV. There are two kinds of Cherenkov telescopes: water Cherenkov telescopes like Milagro (http://www.lanl.gov/milagro/) and atmospheric Cherenkov telescopes, such as MAGIC, H.E.S.S., Whipple, Cangaroo-III (http://wwwmagic.mppmu.mpg.de/links/) and VERITAS (http://veritas.sao.arizona.edu/), and their advanced generations, like MAGIC-II (http://wwwmagic.mppmu.mpg.de/introduction/magic2.html) and H.E.S.S.-II.

Milagro is a TeV gamma-ray detector locating in northern New Mexico operating in the energy band > 100 GeV. It uses the water Cherenkov technique to detect ex-

TABLE I: LAT Specifications and Performance Compared with EGRET (from http://glast.gsfc.nasa.gov/science/instruments/table1-1.html) and GRID (from [27]).

Quantity	LAT	EGRET	GRID
Performance period (year)	2008−?	1991−2000	2006−?
Energy Range	0.02− 300 GeV	0.02 − 30 GeV	0.03−50GeV
Peak Effective Area	$\sim 10^4$ cm^2	1500 cm^2	700 cm^2
Field of View	2.5 sr	0.5 sr	3 sr
Angular Resolution	$< 3.5^0$ at 0.1GeV	5.8^0 at 0.1GeV	4.7^0 at 0.1GeV

tensive air-showers produced by very high energy (VHE) gamma rays as they interact with the Earth's atmosphere. The Milagro field of view is $\sim$ 2 sr and duty cycle is $> 90\%$. The effective area is a function of zenith angle and ranges from 50m^2 at 100 GeV to 10^5 m^2 at 10 TeV [28].

Among the atmospheric Cerenkov telescopes, MAGIC may be best suited for the detection of the prompt emission of GRBs, because of its low energy threshold, its large effective area, and in particular, its capability for fast slewing [29]. The low trigger threshold, currently 50 GeV at zenith, should allow the detection of GRBs even at a redshift $z \sim 1$, as lower energy radiation can effectively reach Earth without interacting much with the diffusive infrared background (see section II B for details). Moreover, in its fast slewing mode, MAGIC can be repositioned within 30 s to any position on the sky; in case of a target-of-opportunity alert by GCN, an automated procedure takes only few seconds to terminate any pending observation, validate the incoming signal, and start slewing toward the GRB position. So far, the maximal repositioning time has been $\sim$ 100 s [29]. In its current configuration, the MAGIC photomultiplier camera has a field of view of 2.0^0 diameter and a peak collection area for $\gamma-$rays of the order of 10^5 m^2 (see the lower panel of Fig.1) [29].

The H.E.S.S. array is a system of four 13m-diameter IACTs located at 1 800 m above sea level. The effective collection area increases from $\sim 10^3$m^2 at 100 GeV to more than 10^5m^2 at 1 TeV, for observations at zenith angles of ≤ 20 deg [30]. The slew rate of the array is $\sim 100^0$ per minute, enabling it to point to any sky position within 2 minutes [30].

VERITAS is a new major ground-based gamma-ray observatory with an array of four 12m optical reflectors for gamma-ray astronomy in the energy range of 50 GeV − 50 TeV band (with maximum sensitivity from 100 GeV to 10 TeV). The telescope design is based on the design of the existing 10m gamma-ray telescope of the Whipple Observatory. In the energy range from 100 GeV to 30 TeV, VERITAS's effective area rises from around 3×10^3 m^2 to well over 10^5 m^2 and its energy resolution is $10-20\%$ [31]. Its slew rate is similar to that of H.E.S.S..

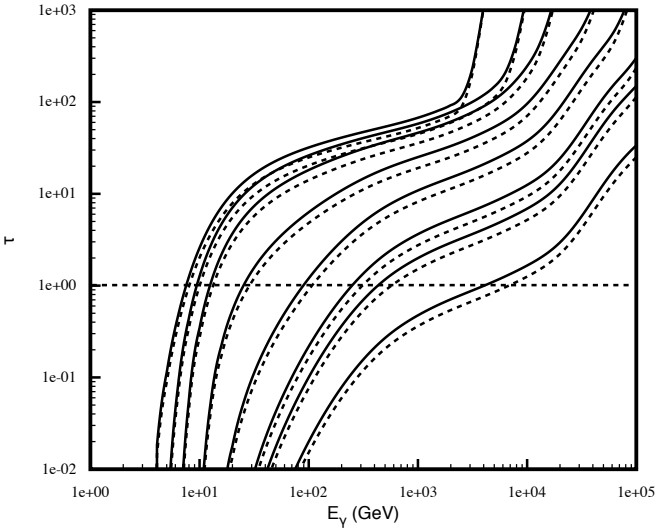

FIG. 2: Optical depth of the universe to γ-rays from interactions with photons of the intergalactic background light (IBL) and CMB for γ-rays having energies up to 100 TeV. The solid lines are for the fast evolution IBL cases, and the dashed lines are for the baseline IBL cases. From bottom to top the curves correspond to redshift $z = (0.03,\ 0.117,\ 0.2,\ 0.5,\ 1,\ 2,\ 3,\ 5)$, respectively (from [34]).

B. Cosmic Attenuation

As $\gamma-$rays with an energy above tens GeV travel toward the observer, they are absorbed due to the interactions with the diffuse infrared background [32, 33]. The probability of a high energy $\gamma-$ray with an energy ϵ_γ to reach earth without being absorbed is $\exp(-\tau)$, where τ can be parameterized by

$$\log \tau = Ax^4 + Bx^3 + Cx^2 + Dx + E,$$

$x \equiv \log(\epsilon_\gamma/1\text{eV})$ and the coefficients, that approximate the lines in Fig.2, have been presented in Table II [34, 35]. For $z \sim 1$ and $\epsilon_\gamma \sim 100$ GeV, we have $\tau \sim 6$, which limits the detection prospect of the VHE emission from GRBs. The spectral energy distribution of intergalactic background light (IBL), particularly at redshift $z > 0.2$, is uncertain. So is the estimate of τ. In some models, for $z \sim 1$ and $\epsilon_\gamma \sim 100$ GeV, a $\tau \sim 1$ is predicted [36] (their recent estimate, however, gives a $\tau \sim 3.3$). If correct, the detection prospect of VHE photons from GRBs will be more promising. The VHE detection of GRBs will

TABLE II: Coefficients for the Baseline IBL (upper low) and Fast Evolution IBL Fits (lower low). The parametric approximation holds for $10^{-2} < \tau < 10^2$ and $\epsilon_\gamma \leq 2$ TeV for all redshifts but also up to 10 TeV for redshifts $z \leq 1$ (from [35]).

z	A	B	C	D	E
0.03	-0.020228	1.28458	-29.1498	285.131	-1024.64
	-0.020753	1.31035	-29.6157	288.807	-1035.21
0.117	0.010677	-0.238895	-1.004	54.1465	-313.486
	0.022352	-0.796354	8.95845	-24.8304	-79.0409
0.2	0.0251369	-0.932664	11.4876	-45.9286	-12.1116
	0.0258699	-0.960562	11.8614	-47.9214	-8.90869
0.5	-0.0221285	1.31079	-28.2156	264.368	-914.546
	0.0241367	-0.912879	11.7893	-54.9018	39.2521
1.0	-0.175348	8.42014	-151.421	1209.13	-3617.51
	-0.210116	10.0006	-178.308	1412.01	-4190.38
2.0	-0.311617	14.5034	-252.81	1956.45	-5671.36
	-0.397521	18.3389	-316.916	2431.84	-6991.04
3.0	-0.34995	16.0968	-277.315	2121.16	-6077.41
	-0.344304	15.8698	-273.942	2099.29	-6025.38
5.0	-0.321182	14.6436	-250.109	1897.00	-5390.55
	-0.28918	13.2673	-227.968	1739.11	-4969.32

provide a significant source sample for studies of IBL as a function of look-back time [37].

C. Observation of high energy prompt emission

EGRET had detected more than 30 GRBs with high energy photon emission [17, 18, 19, 20, 21, 22, 23]. Some of these > 30 MeV photons are simultaneous with the keV−MeV emission, i.e, they are prompt high energy emission.

GRB 940217 is a good example [21]. This burst was detected by the Compton Telescope (COMPTEL), EGRET, Burst And Transient Source (BATSE) and Ulysses. The blue line in Fig.3 is the Ulysses 25−150 keV light curve. The prompt soft $\gamma-$ray emission was clearly visible in a timescale of ~ 180 s (i.e, phase-1). Simultaneously, 10 photons ranging from 40 MeV to 3.4 GeV were recorded. The count rate of these photons is much higher than that of phase-2, the high energy afterglow.

Milagrito observation of GRB 970417A at energies above ~ 0.1 TeV hinted at a distinct higher-energy component (at 3σ level), but lacked energy resolution to provide a spectrum [39]. The excess had a chance probability of 2.8×10^{-5} of being a fluctuation of the background (one detection in 54 bursts). Milagro observed more than 50 GRBs but got null results. The Milagro 99% confidence upper limit on the $0.2-20$ TeV fluence ranges from 10^{-7} to 10^{-3} erg cm^{-2} [28]. Null results at lower energies are also reported by MAGIC observations [40].

The null results at ≥ 100 GeV are not surprising because of the huge absorption of such high energy $\gamma-$rays by the fireball (see eq.(50) below) and by the diffusive infrared background, as already mentioned in section II B.

D. Observation of high energy afterglow

In several GRBs, photons above 30 MeV have arrived after the end of the prompt keV−MeV emission. These are classified as high energy afterglow. It is very interesting to note that the afterglow emission has been first detected in this energy range rather than in X-ray/optical/radio bands even though in low energy bands the photons are more abundant by a factor of $10^3 - 10^6$.

The two best known high energy afterglows are those associated with GRB 940217 and GRB 941017.

GRB 940217: The prompt soft and hard $\gamma-$ray emission has been described in the last subsection. As the 25−150 keV emission ceased, the hard $\gamma-$ray emission did not and lasted longer than 5400 s, including an 18 GeV photon that arrived about an hour after the trigger (see the green circles in phase-2 of Fig.3). In total 18 high energy photons have been detected. The total number could have been higher (probably around 100) if the source was not occulted by the earth for ~ 3700 s after the burst. Note that the 18 GeV photon was observed after the satellite came out from the earth occultation. This high energy afterglow is also characterized by: (a) The count rate of high energy photons seemed to be constant; (b) Except of one photon with an extremely high energy ~ 18 GeV, the energy of the others is nearly a constant, i.e., ~ 100 MeV.

GRB 941017: GRB941017 is one of highest fluence bursts observed by BATSE in its 9-yr lifetime. Ninety per cent of the flux observed by BATSE occurred in a time interval of 77 s. The high-energy component carried at least 3 times more energy than the lower energy component and it lasted about 3 times longer [23]. As shown in Fig.4, there are two additional amazing observation facts: (1) While the soft $\gamma-$ray emission became weaker and weaker and disappeared, both the spectrum and the flux of the hard $\gamma-$ray emission (up to an energy > 200 MeV) were almost constant over a timescale of ~ 200 s; (2) The spectrum of the high energy emission component is rather hard, $F_\nu \propto \nu^0$ where ν is the observed frequency of the photon. The peak energy of the hard component is likely to be above 200 MeV.

Some ground-based Cherenkov detectors have been used to observe the VHE afterglow emission of GRBs. After several years' of search, no evidence for afterglow photons at such high energies has been found [29, 41, 42].

III. PHYSICAL PROCESSES

We focus on relativistic collisionless shocks. Magnetic energy dissipation, for example via magnetic reconnection, can also accelerate the particles and then give rise to prompt [43, 44, 45, 46] and afterglow emission [47, 48].

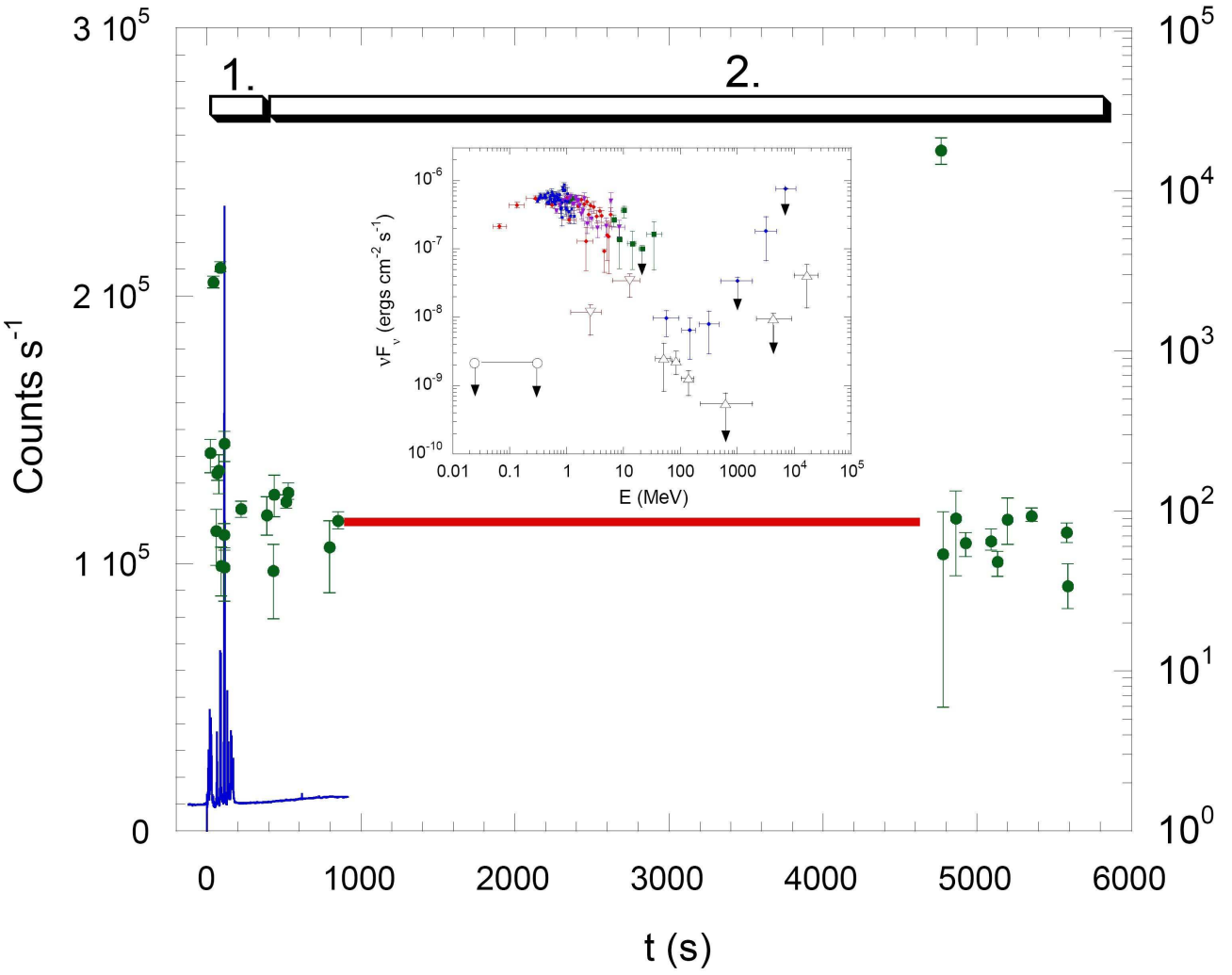

FIG. 3: The prompt keV−GeV $\gamma-$ray emission (i.e., phase-1) and the long lasting high energy afterglow emission (i.e., phase-2) of GRB 940217 (from [38]). The source was earth-occulted for ~ 3700 s and the spectrum of all photons is inserted.

However in this case we expect that the inverse Compton emission will be weak because of the strong magnetic field (see eq.(22) below) and it would not give rise to a significant high energy emission.

In all scenarios that are considered in this review, the emitting material has been accelerated and it moves relativistically relative to central engine with a bulk Lorentz factor Γ. Consequently there are two inertial frames: the rest frame of the emitting region (the comoving frame), and the rest frame of the central engine. The observer's rest frame is the same as the latter aside from a cosmological redshift factor (see also [13]). We denote parameters measured in the comoving frame with the superscript "$'$". The physical quantities (e.g. scale length and time) as viewed in the two inertial frames are related via the Lorentz transformations. Along the emitting region's moving direction in the central engine's frame, the length scales Δ' and Δ, and the time intervals elapsed for the same pair of events dt' and $d\hat{t}$ are related by

$$\Delta' = \Gamma\Delta, \quad dt' = d\hat{t}/\Gamma.$$

$\hat{t}$ is the time measured in the central engine frame. This time is not that useful as we will be generally interested in the observer's time, that is the arrival time of photons as seen by an observer at infinity. For matter moving directly towards the observer the arrival time of a photon emitted at R relative to a photon emitted at $R = 0$ is:

$$t_{\rm obs} = \int_0^R (1-\beta_\Gamma)\frac{dr}{c} \approx \frac{R}{2\Gamma^2 c}, \qquad (1)$$

where $\beta_\Gamma = (1-1/\Gamma^2)^{-1/2}$. A general form $(1-\beta_\Gamma\cos\theta)$ should be used in the integral above if the motion is at an angle θ towards the observer. Since all observations are done with $t_{\rm obs}$ we will use hereafter this observer time and drop the subscript "obs" so $t = t_{\rm obs}$. A cosmological

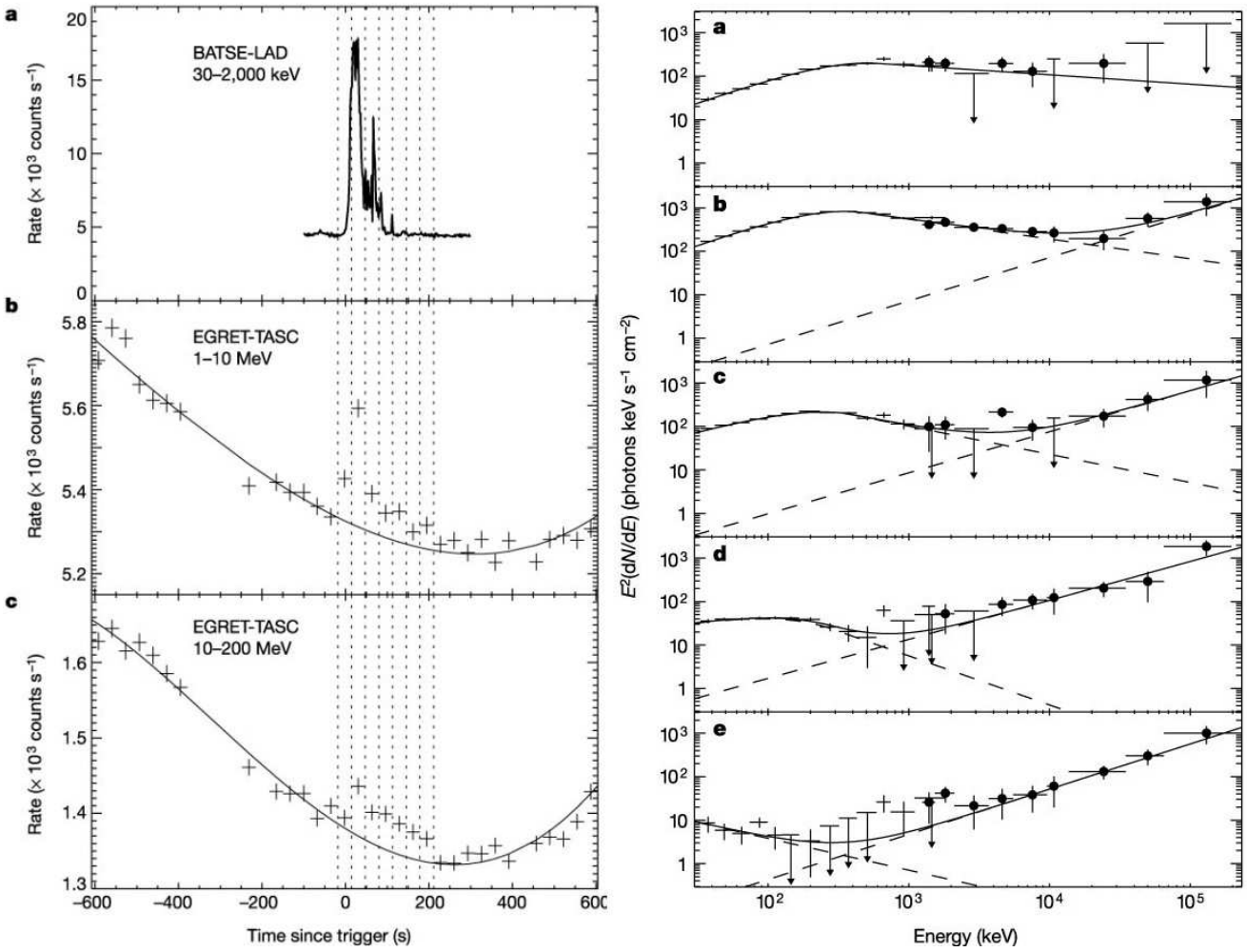

FIG. 4: The keV-GeV $\gamma-$ray light curve (left panel) and spectrum (right panel) of GRB 941017 in five time intervals from -18 s to 211 s (from [23]).

facto (1+z) should be added to the above relation, as appropriate. Note that we have (for $\beta_\Gamma = \text{const.}$)

$$\hat{t}/2\Gamma^2 = t'/\Gamma = t. \tag{2}$$

A. Relativistic shocks

Shocks involve sharp jumps in the physical conditions. Conservation of mass, energy, and momentum determine the Hugoniot shock jump conditions across the relativistic shocks. For the perpendicular shocks, if the upstream matter is cold and magnetized, the jump conditions read [49]

$$\frac{n'_{\rm d}}{n'_{\rm u}} \approx \gamma_{\rm ud}\frac{7+\chi+\sqrt{1+14\chi+\chi^2}}{1+\chi+\sqrt{1+14\chi+\chi^2}}, \tag{3}$$

$$\frac{e'_{\rm d}}{n'_{\rm d}m_{\rm p}c^2} \approx \frac{\gamma_{\rm ud}(1+\sigma)}{8}(7+\chi+\sqrt{1+14\chi+\chi^2})\,[1-\frac{6\chi}{1+\chi+\sqrt{1+14\chi+\chi^2}}], \tag{4}$$

$$\frac{B'_{\rm d}}{B'_{\rm u}} = k\frac{n'_{\rm d}}{n'_{\rm u}}, \tag{5}$$

where $n'_{\rm u,d}$, $e'_{\rm u,d}$ and $B'_{\rm u,d}$ are the number density, the energy density and the magnetic field measured in the local rest framed of the upstream (region u) and downstream (region d), $\gamma_{\rm ud}$ is the Lorentz factor of region u relative to region d, $\chi \equiv \frac{k^2\sigma}{1+\sigma}$, $0 \le k \le 1$ is the parameter describing the magnetic energy dissipation at the shock front ($k = 1$ for the ideal MHD limit) and σ is the ratio of the magnetic energy density to the particle energy density measured in the rest frame of the region u.

For the un-magnetized upstream (i.e., $\sigma = 0$), we have

[50]

$$\frac{n'_{\rm d}}{n'_{\rm u}} \approx 4\gamma_{\rm ud}, \quad \frac{e'_{\rm d}}{n'_{\rm d}m_{\rm p}c^2} \approx \gamma_{\rm ud} - 1. \tag{6}$$

The fraction of thermal energy and the magnetic field behind the shock are needed to calculate the radiation spectrum. These parameters are determined by the microscopic physical processes and are hard to estimate from first principles [8]. A phenomenological approach is to define two dimensionless parameters, $\varepsilon_{\rm B}$ and $\varepsilon_{\rm e}$, that incorporate our ignorance and uncertainties [51]. So the energy of the shock given to the electrons and electrons are

$$U'_e \equiv 4\varepsilon_{\rm e}\gamma_{\rm ud}(\gamma_{\rm ud}-1)n'_{\rm u}m_{\rm p}c^2$$

and

$$U'_{\rm B} \equiv 4\varepsilon_{\rm B}\gamma_{\rm ud}(\gamma_{\rm ud}-1)n'_{\rm u}m_{\rm p}c^2$$

respectively.

B. Particle acceleration

Particle acceleration can occur in GRB blast waves through a First-order Fermi mechanism involving internal or external shocks, and through second-order Fermi acceleration involving gyroresonant scattering of particles by magnetic turbulence in the magnetic field of the blast wave. In the First-order Fermi acceleration, the particles are accelerated when they repeatedly cross a shock. Magnetic-field irregularities keep scattering the particles back so that they keep crossing the same shock. Using the relativistic shock jump conditions and kinematic considerations one can find that the energy gain in the first shock crossing is of the order $\gamma^2_{\rm ud}$ [52]. However, subsequent shock crossings are not as efficient and the energy gain is just of order 2 [53]. Repeated cycles of this type (in each of which the particles gain a factor of ~ 2 in energy) lead to a power-law spectrum with $p \sim 2.3$ for $\gamma_{\rm ud} \gg 1$ [54]. The Second-order Fermi acceleration can work efficiently if magnetic turbulence in the magnetic field of the blast wave has been well developed [55]. Again, the accelerated spectrum could be a power-law with an index $p \sim 2.2$ [56]. In both scenarios, the maximal energy of the protons, limited by the strength of the shocks and the synchrotron cooling, might be as high as $\sim 10^{20}$ eV [52, 55, 57].

As mentioned above, in the shock front, $\varepsilon_{\rm e}$ fraction of shock energy has been given to the fresh electrons swept by the blast wave. If the fresh electrons have a power-law energy distribution $dn'/d\gamma'_e \propto (\gamma'_e - 1)^{-p}$ for $\gamma'_m \le \gamma'_e \le \gamma'_{\rm M}$, with the shock jump conditions that $\int_{\gamma'_m}^{\gamma'_{\rm M}}(dn'/d\gamma'_e)d\gamma'_e = n'_{\rm d}$ and $\int_{\gamma'_m}^{\gamma'_{\rm M}}(\gamma'_e - 1)m_{\rm e}c^2(dn'/d\gamma'_e)d\gamma'_e = U'_{\rm e}$, we have

$$\gamma'_m \approx \varepsilon_{\rm e}(\gamma_{\rm ud}-1)\frac{p-2}{p-1}\frac{m_{\rm p}}{m_e} + 1, \tag{7}$$

where the maximal Lorentz factor is limited by the synchrotron losses and is given by [58]

$$\gamma'_{\rm M} \approx (\frac{3e}{B'\sigma_{\rm T}})^{1/2} \approx 4\times 10^7 B'^{-1/2}, \tag{8}$$

where e and $\sigma_{\rm T}$ are the charge and the Thompson cross section of electrons, respectively. The magnetic field strength

$$\begin{aligned} B' &= \sqrt{8\pi U'_{\rm B}} = \sqrt{32\pi\varepsilon_{\rm B}\gamma_{\rm ud}(\gamma_{\rm ud}-1)n'_{\rm u}m_{\rm p}c^2} \\ &\approx 0.04(\frac{\varepsilon_{\rm B}}{0.01})^{1/2} {n'_{\rm u}}^{1/2}\gamma_{\rm ud}\beta_{\rm ud}\ \text{Gauss}, \end{aligned} \tag{9}$$

where $\beta_{\rm ud} = \sqrt{1-1/\gamma^2_{\rm ud}}$. So in the internal shocks or the early forward shock, B' is larger or even significantly larger than 1 Gauss as $n'_{\rm u} \gg 1$ in internal shocks and $\gamma_{\rm ud} \sim \Gamma \gg 1$ in the early forward shock.

C. Radiation processes

1. *Synchrotron radiation*

The typical energy of synchrotron photons as well as the synchrotron cooling time depends on the Lorentz factor of the relativistic electron under consideration and on the strength of the magnetic field. If the emitting region moves with a Lorentz factor Γ, the photons are blue-shifted. The typical photon energy in the observer frame is given by [59]

$$\nu_{\rm syn} = \frac{\mathcal{D}\nu'_{\rm syn}}{1+z} \approx \frac{eB'}{2\pi(1+z)m_{\rm e}c}{\gamma'_e}^2\Gamma, \tag{10}$$

where $\mathcal{D} \equiv [\Gamma(1-\beta_\Gamma\cos\theta)]^{-1}$.

The power emitted, in the comoving frame, by a single electron due to synchrotron radiation is [59]

$$P'_{\rm syn} = \frac{4}{3}\sigma_{\rm T}cU'_{\rm B}({\gamma'_e}^2 - 1). \tag{11}$$

The synchrotron cooling time of an electron with a Lorentz factor γ'_e is $t'_c \approx \gamma'_e m_{\rm e}c^2/P'_{\rm syn}$. If t'_c is smaller than the dynamical time $t'_d \approx R/\Gamma c$, the electron cools rapidly (i.e., *fast cooling*), where R is the radius of the shock front to the central engine. We thus can define the cooling Lorentz factor of the shocked electrons (γ'_c, which satisfies $t'_c = t'_d$) as

$$\gamma'_c \approx \frac{6\pi\Gamma m_{\rm e}c^2}{\sigma_{\rm T}RB'^2}.$$

If $\gamma'_c > \gamma'_m$, the cooling of most electrons are not very fast, we call this case as *slow cooling*. The synchrotron radiation of electrons in turn modify their isotropic-equivalent energy distribution $N_{\gamma'_e}$. The continuity equation of electrons reads

$$\frac{\partial N_{\gamma'_e}}{\partial t'} + \frac{\partial}{\partial\gamma'_e}(N_{\gamma'_e}\frac{d\gamma'_e}{dt'}) = Q, \tag{12}$$

where $\frac{d\gamma'_e}{dt'} \approx -\frac{\sigma_{\rm T}B^2}{6\pi m_e c}{\gamma'_e}^2$ and $Q \propto {\gamma'_e}^{-p}$ for $\gamma'_m \leq \gamma'_e \leq {\gamma'}_{\rm M}$.

For a stationary distribution, $\frac{\partial N_{\gamma'_e}}{\partial t'} = 0$. We thus have $\frac{\partial}{\partial\gamma'_e}(N_{\gamma'_e}\frac{d\gamma'_e}{dt'}) = Q$. In both the fast and slow cooling cases, the electrons having a $\gamma'_e > \gamma'_c$ get cooled rapidly, for which the distribution should be $N_{\gamma'_e} \propto (d\gamma'_e/dt')^{-1}\int Q d\gamma'_e \propto {\gamma'_e}^{-(p+1)}$. For $\gamma'_m < \gamma'_e < \gamma'_c$, the cooling is unimportant so the distribution is still $\propto Q \propto {\gamma'_e}^{-p}$. For $\gamma'_c < \gamma'_e < \gamma'_m$, we have $Q = 0$ and then $N_{\gamma'_e} \propto {\gamma'_e}^{-2}$. Overall, we have the following distributions:

$$N_{\gamma'_e} \propto \begin{cases} {\gamma'_e}^{-(p+1)}, & \text{for } \gamma'_e > \max\{\gamma'_c,\ \gamma'_m\}, \\ {\gamma'_e}^{-p}, & \text{for } \gamma'_c > \gamma'_e > \gamma'_m, \\ {\gamma'_e}^{-2}, & \text{for } \gamma'_m > \gamma'_e > \gamma'_c. \end{cases} \quad (13)$$

The synchrotron radiation spectrum can be easily estimated. The spectrum of one electron moving in a magnetic field B' can be approximated by

$$F'(x) \approx 2.149\frac{\sqrt{3}e^3B'}{m_e c^2}x^{1/3}e^{-x}, \quad (14)$$

where $x \equiv \nu'/\nu'_{\rm syn}$ and $\nu' = (1+z)\mathcal{D}^{-1}\nu$ (ν is the observer's frequency). We see that $F'(x)$ peaks at $x = 1/3$. If the synchrotron self-absorption is unimportant, for $\nu < \min\{\nu_c,\ \nu_m\}$, the emission is the sum of the contributions of the tails of all the electrons' emissions $F_\nu \propto \nu^{1/3}$, where $\nu_c \equiv \nu_{\rm syn}(\gamma'_c)$ and $\nu_m \equiv \nu_{\rm syn}(\gamma'_m)$. In higher energy range, using $F_\nu d\nu \propto N_{\gamma'_e}P'_{\rm syn}d\gamma'_e$ and $\nu \propto {\gamma'_e}^2$, we have $F_\nu \propto \nu^{-1/2}$ for $\nu_c < \nu < \nu_m$, $F_\nu \propto \nu^{-(p-1)/2}$ for $\nu_m < \nu < \nu_c$ and $F_\nu \propto \nu^{-p/2}$ for $\max\{\nu_m,\ \nu_c\} < \nu$. In summary, the synchrotron radiation spectrum can be approximated as (see also [60])

$$F_{\nu,\rm syn} \propto \begin{cases} \nu^{-p/2}, & \text{for } \nu_{\rm M} > \nu > \max\{\nu_c,\ \nu_m\}, \\ \nu^{-(p-1)/2}, & \text{for } \nu_c > \nu > \nu_m, \\ \nu^{-1/2}, & \text{for } \nu_m > \nu > \nu_c, \\ \nu^{1/3}, & \text{for } \min\{\nu_c,\ \nu_m\} > \nu. \end{cases} \quad (15)$$

The maximal specific flux is estimated as [60, 61]

$$F_{\nu,\rm syn-max} \approx \frac{(1+z)e^3N_{e,\rm tot}\Gamma B'}{4\pi m_e c^2 D_L^2},$$

where $N_{e,\rm tot}$ is the total number of electrons and D_L is the luminosity distance of the emitting source.

The maximal synchrotron frequency can be estimated by comparing the synchrotron cooling time with the acceleration time [58]

$$\begin{aligned} h\nu_{\rm M} &= \frac{\mathcal{D}h\nu'_{\rm M}}{1+z} \approx \frac{heB'}{2\pi(1+z)m_{\rm e}c}{\gamma'}^2_{\rm M}\Gamma \\ &\approx \frac{9hm_ec^3}{16(1+z)\pi^2e^2}\Gamma \approx \frac{30\Gamma}{1+z}\ {\rm MeV}. \end{aligned} \quad (16)$$

In the prompt emission phase, $\Gamma \sim 100$, we have $h\nu_{\rm M} \sim$ a few GeV. In the early afterglow phase, $h\nu_{\rm M} \sim 10 - 100$ MeV. If more energetic photons have been observed, other mechanism(s) should be present.

Protons can also produce synchrotron emission but this is, of course, much weaker as for $\gamma'_{\rm p} = \gamma'_e$, the synchrotron radiation power of a proton is weaken by a factor of $(m_{\rm e}/m_{\rm p})^2$ of an electron. We assume an initial power-law distribution $dn'/d\gamma'_{\rm p} \propto (\gamma'_{\rm p} - 1)^{-p}$, for protons accelerated in the blast wave, the minimum Lorentz factor, the cooling Lorentz factor and the Maximum Lorentz factor are

$$\gamma'_{\rm m,p} = (1 - \varepsilon_{\rm e} - \varepsilon_{\rm B})(\gamma_{\rm ud} - 1)(p-2)/(p-1) + 1,$$

$$\gamma'_{\rm c,p} \approx \frac{6\pi\Gamma m_{\rm p}c^2}{\sigma_{\rm T,p}RB'^2} \approx (\frac{m_{\rm p}}{m_{\rm e}})^3\gamma'_c,$$

$$\gamma'_{\rm M,p} \approx (m_p/m_e)\gamma'_{\rm M},$$

respectively, where the Thompson cross section of protons is $\sigma_{\rm T,p} = (m_{\rm e}/m_{\rm p})^2\sigma_{\rm T}$. For $\gamma'_{\rm c,p} > \gamma'_{\rm M,p}$, we take $\gamma'_{\rm c,p} = \gamma'_{\rm M,p}$. The synchrotron radiation frequency of the protons is

$$\nu_{\rm syn,p} = \frac{\mathcal{D}\nu'_{\rm syn,p}}{1+z} \approx \frac{eB'}{2\pi(1+z)m_{\rm p}c}{\gamma'_{\rm p}}^2\Gamma.$$

With $\nu_{m,\rm p} = \nu_{\rm syn,p}(\gamma'_{m,\rm p})$, $\nu_{\rm c,p} = \nu_{syn,p}(\gamma'_{c,\rm p})$ and $\nu_{\rm M,p} = \nu_{syn,p}(\gamma'_{\rm M,p})$, it is straightforward to obtain the spectra, which take the form of eq.(15). We note that

$$\nu_{\rm M,p} \sim (m_{\rm p}/m_{\rm e})\nu_{\rm M}$$

could be in TeV [62]. But for reasonable shock parameters that fit the afterglow data, the synchrotron TeV emission of protons is not as important as that of the synchrotron-self Compton of electrons [63]. In this review, we do not discuss it any more.

2. *Inverse Compton scattering*

An electron moving relative to a dense soft photon background will lose some of its energy via inverse Compton scattering [59] and produce an inverse Compton component at higher energies

$$\nu_{\rm ic} = \frac{\mathcal{D}\nu'_{\rm ic}}{1+z} \approx \frac{2\Gamma}{1+z}\frac{{\gamma'_e}^2\nu'_{\rm se}}{1+g}, \quad (17)$$

where $\nu'_{\rm se}$ is the frequency of the seed photon and $g \equiv \gamma'_e h\nu'_{\rm se}/m_{\rm e}c^2$.

In the Thompson regime, $g \ll 1$, so

$$\nu'_{\rm ic} \approx {\gamma'_e}^2\nu'_{\rm se}. \quad (18)$$

In the Klein-Nishina regime, $g \geq 1$, we have

$$\nu'_{\rm ic} \approx \gamma'_e m_{\rm e}c^2/h. \quad (19)$$

In this case, apart from the reduction in energy boost, the cross-section for scattering is also reduced to [59]

$$\sigma(\nu'_{\rm se},\gamma'_e)=\frac{3}{4}\sigma_T\{\frac{(1+g)}{g^3}\left[\frac{2g(1+g)}{(1+2g)}-\ln(1+2g)\right]+\frac{1}{2g}\ln(1+2g)-\frac{(1+3g)}{(1+2g)^2}\}. \quad (20)$$

For convince, we define $A(g)\equiv\sigma(\nu'_{\rm se},\gamma'_e)/\sigma_{\rm T}$.

The effect of inverse Compton scattering depends on the parameter

$$Y_{\rm ic}\equiv P'_{\rm ic}/P'_{\rm syn}, \quad (21)$$

where $P'_{\rm ic}$ is the power of the inverse Compton radiation, which can be estimated as $P'_{\rm ic}\approx A(g)\sigma_{\rm T}c({\gamma'_e}^2-1)U'_\gamma/(1+g)$, where U'_γ is the energy density of the seed photons. We then have [64]

$$Y_{\rm ic}\approx\frac{A(g)}{1+g}\frac{U'_\gamma}{U'_{\rm B}}\approx\frac{U'_\gamma}{U'_B}\begin{cases}1, & \text{for } g\ll 1,\\ \frac{1}{g^2}, & \text{for } g\gg 1.\end{cases} \quad (22)$$

If $Y_{\rm ic}<1$, the inverse Compton effect is unimportant and can be ignored. On the other hand if $Y_{\rm ic}>1$ IC is important. Note that second order IC will be even more important (see eq.(36) below) and so will even higher orders. This divergence will be stopped by the Klien-Nishina cutoff.

In general

$$P'_{\rm ic}(\gamma'_e)=\int_0^\infty h\nu'_{\rm ic}\frac{dN'_\gamma}{dt'd\nu'_{\rm ic}}d\nu'_{\rm ic}. \quad (23)$$

The quantity $dN'_\gamma/dt'd\nu'_{\rm ic}$ is the scattered photon spectrum per electron [65]. Supposing the seed photons are isotropic in the rest frame of the IC scattering region, we can express $dN'_\gamma/dt'd\nu'_{\rm ic}$ as (see eq.(37) for anisotropic photons):

$$\frac{dN'_\gamma}{dt'd\nu'_{\rm ic}}=\frac{3\sigma_T c}{4{\gamma'_e}^2}\frac{n'_{\nu'_{\rm se}}d\nu'_{\rm se}}{\nu'_{\rm se}}[2q\ln q+(1+2q)(1-q)+\frac{1}{2}\frac{(4gq)^2}{1+4gq}(1-q)], \quad (24)$$

where $f\equiv h\nu'_{\rm ic}/(\gamma'_e m_e c^2)$ satisfying $h\nu'_{\rm se}/(\gamma'_e m_e c^2)\le f\le 4g/(1+4g)$, $q\equiv f/[4g(1-f)]$, and $n'_{\nu'_{\rm se}}$ is the frequency distribution of the seed photons in unit volume [65, 66].

The cooling of electrons caused by synchrotron and IC radiation and adiabatic cooling is described by

$$\frac{d\gamma'_e}{dR}=-\frac{4\sigma_{\rm T}}{3m_{\rm e}c^2}\frac{U'_B}{\beta_\Gamma\Gamma}[1+Y_{\rm ic}]{\gamma'_e}^2-\frac{\gamma'_e}{R}, \quad (25)$$

where $dR\approx\Gamma\beta_\Gamma c dt'$. Correspondingly, the cooling Lorentz factor takes a new form

$$\gamma'_c=\frac{6\pi\Gamma m_{\rm e}c^2}{(1+Y_{\rm ic})\sigma_{\rm T}RB'^2}, \quad (26)$$

which is used throughout the rest of the review.

Considering the spherical curvature of the emitting region, the observed IC emission flux is

$$\begin{aligned}F_{\nu_{\rm ic}} &= \frac{(1+z)}{16\pi^2D_L^2}\int\mathcal{D}^3h\nu'_{\rm ic}\frac{dN'_\gamma}{dt'd\nu'_{\rm ic}}N_{\gamma'_e}d\gamma'_e d\Omega\\ &\approx \frac{(1+z)\Gamma}{4\pi D_L^2}\int h\nu'_{\rm ic}\frac{dN'_\gamma}{dtd\nu'_{\rm ic}}N_{\gamma'_e}d\gamma'_e, \end{aligned}\quad (27)$$

where Ω is the solid angle.

For electrons having a power-law energy distribution $N_{\gamma'_e}\propto{\gamma'_e}^{-p}$, the IC spectrum is only weakly dependent on $n'_{\nu'_{\rm se}}$ and can be approximated as (see eq.(2.76) and eq.(2.88) of [65] for details)

$$F_{\nu_{\rm ic}}\propto\begin{cases}\nu_{\rm ic}^{-(p-1)/2}, & \text{for } g\ll 1,\\ \nu_{\rm ic}^{-p}, & \text{for } g\gg 1.\end{cases} \quad (28)$$

Following [24], we present two different approaches to calculate the IC scattering with Klein-Nishina suppression self-consistently.

Instantaneous approximation. In this approach we assume a functional form for the energy distribution of the electrons acceleration in the shock front, $n'(\gamma'_e)$, and consider its instantaneous modification due to cooling. An electron of Lorentz factor γ'_e has a cooling time given by

$$t'_c(\gamma_e)\approx\frac{\gamma'_e m_e c^2}{P'_{\rm syn}(\gamma'_e)+P'_{\rm ic}(\gamma'_e)}. \quad (29)$$

If $t'_c(\gamma'_e)\ge t'_d$, then the electron emits both synchrotron and IC radiation for the entire time t'_d. However, when $t'_c(\gamma_e)<t'_d$, the electron radiates only for a time $t'_c(\gamma_e)$. Thus, the total spectral radiation density, including that of the seed photons and that produced by all the electrons in the fluid, is given by:

$$\begin{aligned}U'_{\nu'} &= n'_{\nu'_{\rm se}}h\nu'_{\rm se}\,|_{\nu'_{\rm se}=\nu'}+\int_{\gamma'_{\rm min}}^\infty[P'_{\rm syn}(\nu',\gamma'_e)\\ &+ P'_{\rm ic}(\nu',\gamma'_e)]\times{\rm Min}[t'_d,t'_c(\gamma'_e)]\,n'(\gamma'_e)d\gamma'_e, \end{aligned}\quad (30)$$

where $P'_{\rm syn}(\nu',\gamma'_e) \approx (\sigma_{\rm T} m_{\rm e} c^2 B') F'(\nu'/\nu'_{\rm syn})/3e$ and $P'_{\rm ic}(\nu',\gamma'_e) \approx (1+g) c U'_{\nu'} \sigma(\nu',\gamma'_e)$.

Equation (30) is an integral equation, since the function $P'_{\rm ic}(\nu',\gamma'_e)$ inside the integral itself depends on $U'_{\nu'}$. The quantity $\gamma'_{\rm min}$ is the smallest γ'_e down to which electrons are present. In dealing with equation (30) we need to consider two cases. One is the *slow cooling*, in which we may use equation (30) directly with $\gamma'_{\rm min} = \gamma'_m$ and $n'(\gamma'_e)$ given by the original energy distribution produced in the shock. The other is the *fast cooling*, in which electrons will continue to cool below γ_m to a minimum $\gamma'_{\rm min}$ such that $t'_c(\gamma'_{\rm min}) = t'_d$. Now, for the range $\gamma'_{\rm min} \leq \gamma'_e < \gamma'_m$, all the electrons are available for radiating. Initially, most of the electrons are at γ'_m, and as these electrons cool each electron will pass every γ'_e between γ'_m and $\gamma'_{\rm min}$ (where all these electrons accumulate). Hence we have

$$n'(\gamma'_e) \sim n'(\gamma'_m), \qquad \gamma'_{\rm min} \leq \gamma'_e < \gamma'_m. \tag{31}$$

As usual, we assume a power-law distribution for the electron Lorentz factor $n'(\gamma'_e) d\gamma'_e \propto {\gamma'_e}^{-p} d\gamma'_e$ ($\gamma'_e \geq \gamma'_m$), for which γ'_m is given by eq.(7). Equation (30) may be solved numerically via an iterative method. The algorithm proceeds as follows. We begin with some reasonable initial approximation for $U'_{\nu'}$. Using this, we compute $P'_{\rm ic}(\gamma_e)$, $t'_c(\gamma'_e)$ and $\gamma'_{\rm min}$. Then, we compute the spectral distributions $P'_{\rm syn}(\nu',\gamma'_e)$ and $P'_{\rm ic}(\nu',\gamma'_e)$ for all $\gamma'_e \geq \gamma'_{\rm min}$ and obtain via equation (30) a new approximation for $U'_{\nu'}$. We take this $U'_{\nu'}$, or (for smoother convergence) a suitable linear combination of the new and old $U'_{\nu'}$, as the current approximation for $U'_{\nu'}$ and repeat the steps. The iteration usually converges fairly quickly.

Dynamical approach. In the limit of a single IC scattering, with given $n'_{\nu'_{\rm se}}$, Γ, B' and Q, eq.(12), eq.(21) and eqs.(23-25) form a complete set of formulae which can be solved for $N_{\gamma'_e}$ numerically. Then the IC flux can be obtained using eq.(27). The treatment is a bit more complicated if the synchrotron radiation component $n'_{\nu'_{\rm s}} \approx \int_3^{\gamma'_{\rm M}} \frac{1}{h\nu'_{\rm s}} \frac{N_{\gamma'_e}}{4\pi R^2 c} F'(\nu'_{\rm s}/\nu'_{\rm syn}) d\gamma'_e$ (see eq.(14) for $F'(\nu'/\nu'_{\rm syn})$) is comparable to the seed photon background. In this case we need to replace the term $n'_{\nu'_{\rm se}}$ in eq.(24) by $n'_{\nu'_{\rm se}} + n'_{\nu'_{\rm s}}|_{\nu'_{\rm s}=\nu'_{\rm se}}$ and then solve for $N_{\gamma'_e}$ self-consistently. The resulting $n'_{\nu'_{\rm ic}} \equiv \int \frac{dN'_\gamma}{dt' d\nu'_{\rm ic}} \frac{N_{\gamma'_e}}{4\pi R^2 c} d\gamma'_e$ in turn plays an role in cooling the electrons. Combining this IC component with $n'_{\nu'_{\rm se}}$ and the synchrotron radiation component of electrons, we can solve for $N_{\gamma'_e}$ self-consistently and then calculate the second order IC spectrum and so on.

Synchrotron-self Compton (SSC) takes place if the seed photons involved in the inverse Compton scattering are the synchrotron radiation of the shock-accelerated electrons (i.e., $U'_\gamma = U'_{\rm syn}$). In the comoving frame of the shocked material, both the electrons and the seed photons are isotropic. The Synchrotron-self Compton parameter $Y_{\rm ssc}$ can be estimated as

$$Y_{\rm ssc} \approx \frac{A(g)}{1+g} \frac{U'_{\rm syn}}{U'_B} = \frac{A(g)}{1+g} \eta \frac{\varepsilon_{\rm e}}{\varepsilon_{\rm B}} \frac{1}{1+Y_{\rm ssc}}, \tag{32}$$

where $\eta = \min\{1, (\gamma'_m/\gamma'_c)^{p-2}\}$ and the relation $U'_{\rm syn} = \eta U'_e/(1+Y_{\rm ssc})$ has been taken into account. In the Thompson regime, we have [67]

$$\begin{aligned} Y_{\rm ssc} &\approx \frac{-1+\sqrt{1+4\eta\varepsilon_{\rm e}/\varepsilon_{\rm B}}}{2} \\ &\approx \begin{cases} \eta\varepsilon_{\rm e}/\varepsilon_{\rm B}, & \text{for } \eta\varepsilon_{\rm e}/\varepsilon_{\rm B} \ll 1, \\ (\eta\varepsilon_{\rm e}/\varepsilon_{\rm B})^{1/2}, & \text{for } \eta\varepsilon_{\rm e}/\varepsilon_{\rm B} \gg 1. \end{cases} \end{aligned} \tag{33}$$

The SSC spectrum can be approximated as follows:

$$F_{\nu,\rm ssc} \propto \begin{cases} \nu^{-p/2}, & \text{for } \nu_{\rm M,ssc} > \nu > \max\{\nu_{c,\rm ssc},\ \nu_{m,\rm ssc}\}, \\ \nu^{-(p-1)/2}, & \text{for } \nu_{c,\rm ssc} > \nu > \nu_{m,\rm ssc}, \\ \nu^{-1/2}, & \text{for } \nu_{m,\rm ssc} > \nu > \nu_{c,\rm ssc}, \\ \nu^{1/3}, & \text{for } \nu < \min\{\nu_{c,\rm ssc},\ \nu_{m,\rm ssc}\}, \end{cases} \tag{34}$$

where $\nu_{m,\rm ssc} \approx 2{\gamma'_m}^2 \nu_m$, $\nu_{c,\rm ssc} \approx 2{\gamma'_c}^2 \nu_c$ [68], and the SSC cut-off frequency $\nu_{\rm M,ssc} \sim \frac{\Gamma^2 m_e^2 c^4}{h^2 \max\{\nu_m,\nu_c\}}$, above which the IC is in Klein-Nishina regime and is very weak. With a given synchrotron spectrum $F_{\nu,\rm syn}$ taking the form of eq.(15), the SSC spectrum is fixed by

$$Y_{\rm ssc} \int_{\min\{\nu_c,\nu_m\}}^{\nu_{\rm M}} F_{\nu,\rm syn} d\nu \approx \int_{\min\{\nu_{c,\rm ssc},\nu_{m,\rm ssc}\}}^{\nu_{\rm M,ssc}} F_{\nu,\rm ssc} d\nu. \tag{35}$$

If $\max\{{\gamma'_m}^3\nu_m,\ {\gamma'_c}^3\nu_c\}/\Gamma < m_e c^2/2$, the second order IC scattering is still in Thompson regime. The luminosity ratio is given by

$$Y_{\rm ssc} = \frac{U'_{\rm syn}}{U'_B} = \frac{1}{1+Y_{\rm ic}} \frac{\eta U'_{\rm e}}{U'_B} = \frac{1}{1+Y_{\rm ssc}+Y_{\rm 2ndIC}} \frac{\eta U'_{\rm e}}{U'_B},$$

where $Y_{\rm 2ndIC} = U'_{\rm ssc}/U'_B = (U'_{\rm ssc}/U'_{\rm syn})(U'_{\rm syn}/U'_{\rm B}) = Y^2_{\rm ssc}$, which dominates $Y_{\rm ic}$ if $Y_{\rm ssc} > 1$. For $\eta U'_{\rm e}/U'_{\rm B} = \eta\varepsilon_{\rm e}/\varepsilon_{\rm B} \gg 1$, we have (see also [69, 70])

$$Y_{\rm ssc} \approx (\eta\varepsilon_{\rm e}/\varepsilon_{\rm B})^{1/3}, \quad Y_{\rm 2ndIC} \approx (\eta\varepsilon_{\rm e}/\varepsilon_{\rm B})^{2/3}. \tag{36}$$

Most of the energy of electrons are lost in the second scattering. Now $\nu_{m,\rm 2ndIC} \approx 4{\gamma'_m}^4 \nu_m$ and $\nu_{c,\rm 2ndIC} \approx 4{\gamma'_c}^4 \nu_c$. The spectrum takes the same form of that of eq.(34). Similarly if the third scattering is still in Thompson regime and $\eta\varepsilon_{\rm e}/\varepsilon_{\rm B} \gg 1$, we have $Y_{\rm ssc} \approx (\eta\varepsilon_{\rm e}/\varepsilon_{\rm B})^{1/4}$ and $Y_{\rm 3rdIC} \approx (\eta\varepsilon_{\rm e}/\varepsilon_{\rm B})^{3/4}$.

External inverse Compton (EIC) takes place if the seed photons are from a region well separated from the scattering electrons and along the direction in which the ejecta moves. In this case, the electrons are isotropic but the seed photons, of course, are highly beamed. The spectrum of radiation scattered at an angle $\theta_{\rm sc}$ relative

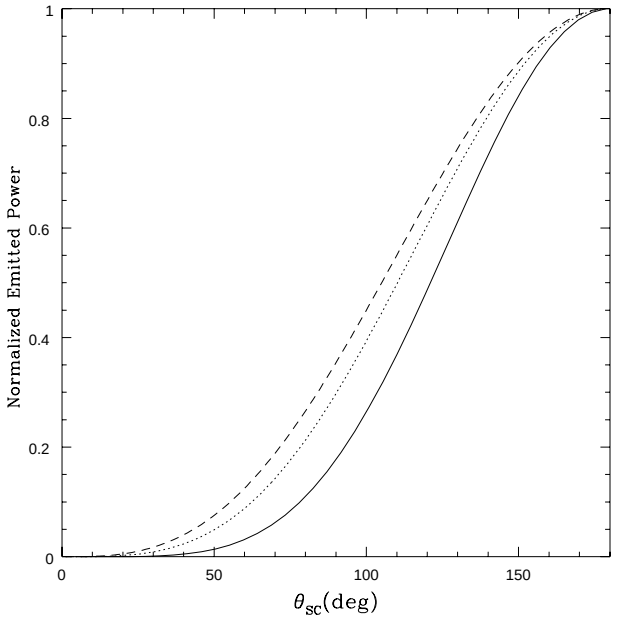

FIG. 5: The normalized emitted power as a function of the scattering angle for different power-law energy distribution electrons (from [72]). From bottom to top, the power-law indexes are 4, 2.5, 2.0 respectively.

to the direction of the photon beam penetrating through this region is [71]:

$$\frac{dN'_\gamma}{dt' d\nu'_{\rm eic} d\Omega'} \approx \frac{3\sigma_T c}{16\pi {\gamma'_e}^2} \frac{n'_{\nu'_{\rm se}} d\nu'_{\rm se}}{\nu'_{\rm se}} [1 + \frac{\xi^2}{2(1-\xi)} - \frac{2\xi}{b_\theta(1-\xi)} + \frac{2\xi^2}{b_\theta^2 (1-\xi)^2}], \quad (37)$$

where $d\Omega' = 2\pi \sin\theta_{\rm sc} d\theta_{\rm sc}$, $\xi \equiv h\nu'_{\rm eic}/(\gamma'_e m_e c^2)$, $b_\theta = 2(1-\cos\theta_{\rm sc})\gamma'_e h\nu'_{\rm se}/(m_e c^2)$, $\cos\theta_{\rm sc} = (\cos\theta - \beta_\Gamma)/(1-\beta_\Gamma \cos\theta)$, and $h\nu'_{\rm se} \ll h\nu'_{\rm eic} \leq \gamma'_e m_e c^2 b_\theta/(1+b_\theta)$. In the case of isotropically distributed photons, the averaging of eq.(37) over the angle $\theta_{\rm sc}$ reduces to eq.(24), as expected.

In the rest frame of the emitting region, the EIC emission has a maximum at $\theta_{\rm sc} = \pi$ and it vanishes for small scattering angles, as shown in Fig.5. This effect lowers the EIC flux in two ways [24]. First, a fraction of the total energy is emitted out of our line of sight and thus the received power is depressed (relative to the isotropic seed photon case). Second and more important for GRB study, the strongest emission is from $\theta \sim 1/\Gamma$ (see eq.(59) below). As a result, the EIC emission duration is extended and the flux is lowered. This will have important implications on EIC from X-ray flares as discussed in section IV A 3 below.

Bulk Compton Scattering. Inverse Compton may arise even if the electrons in the ejecta are cold but are moving relativistically into a soft photon background. In this case, the IC spectrum depends on both the initial spectrum of seed photons and the deceleration of the electrons. Roughly speaking, the upscattered photons have a much larger frequency $\nu_{\rm bic} \sim \Gamma^2 \nu_{\rm se}$ and the flux is $F_{\nu_{\rm bic}} \sim \tau_{\rm bic} F_{\nu_{\rm se}}$, where $\tau_{\rm bic} \sim \sigma_{\rm T} N_{e,{\rm tot}}/(4\pi R^2)$, $\nu_{\rm se}$ is the frequency of the background photons (measured by the observer) and $F_{\nu_{\rm se}}$ is the spectrum.

3. $\gamma-$rays from pion production

High energy photons can also be produced via π^0 decay

$$\pi^0 \rightarrow \gamma + \gamma. \quad (38)$$

In GRB internal shocks and blast waves, π^0 can be produced via the following processes:

$$p+p \rightarrow p+p+\pi^0,\ p+n \rightarrow p+n+\pi^0,\ p+\gamma \rightarrow \Delta^+ \rightarrow \pi^0+p. \quad (39)$$

Please note that in this sub-subsection, p and n represent proton and neutron respectively and γ represents photon. In the rest frame of the outflow, the inelastic pion production threshold is $\epsilon'_{\rm pion} \sim 140$ MeV. For the observer, the resulting $\gamma-$rays thus have an energy $\geq 70\Gamma$ MeV. Actually, the $\gamma-$rays resulting in $p+\gamma \rightarrow \Delta^+ \rightarrow \pi^0+p \rightarrow \gamma+\gamma+p$ are much more energetic because the cross section of $p+\gamma \rightarrow \Delta^+$ peaks when $\epsilon_\gamma \times \epsilon_{\rm proton} \sim (0.3\ {\rm GeV})^2\Gamma^2$, where ϵ_γ is the typical energy of prompt $\gamma-$rays and $\epsilon_{\rm proton}$ is the energy of VHE protons. So we have

$$\epsilon_{\rm proton} \sim 0.1\ \Gamma^2/[\epsilon_\gamma/(1\ {\rm MeV})]\ {\rm TeV}. \quad (40)$$

For the observer, the photons from the π^0-decay is as energetic as $\sim 5\ \Gamma^2/[\epsilon_\gamma/(1\ {\rm MeV})]$GeV if the energy of π^0 is $\sim 10\%$ of the incident protons.

Alternatively, high energy photons are also arise from in the synchrotron radiation of the pairs that result in the $\pi^+,\ \pi^-$ decay

$$\pi^+ \rightarrow \mu^+ + \nu_\mu \rightarrow e^+ + \nu_e + \bar{\nu}_\mu + \nu_\mu.$$
$$\pi^- \rightarrow \mu^- + \bar{\nu}_\mu \rightarrow e^- + \bar{\nu}_e + \nu_\mu + \bar{\nu}_\mu. \quad (41)$$

Possible processes involved in GRBs to produce $\pi^+,\ \pi^-$ are following

$$p+n \rightarrow n+n+\pi^+, \quad p+p \rightarrow p+n+\pi^+.$$
$$p+n \rightarrow p+p+\pi^-.$$
$$p+\gamma \rightarrow \Delta^+ \rightarrow \pi^+ + n. \quad (42)$$

The last process of the above four is particularly interesting because the resulting e^+ has a very high random Lorentz factor $\gamma'_{e^+} \sim 0.05\ \epsilon_{\rm proton}/(\Gamma m_e c^2) \sim 10^4\Gamma/[\epsilon_\gamma/(1\ {\rm MeV})]$. It's synchrotron radiation may peak at TeV energies. Though interesting, the energy of this TeV emission component is not expected to be more than that of the synchrotron soft $\gamma-$ray emission unless $\varepsilon_{\rm e} \leq 0.01$ (e.g., [26]). This is because the fraction of total shock energy given to protons above $\epsilon_{\rm proton} \sim 10^7\ \Gamma_{2.5}^2/[\epsilon_\gamma/(1\ {\rm MeV})]$ GeV is only $\leq 1/3$. Furthermore, only a small fraction (≤ 0.1) of the energy of these ultra-relativistic protons is lost in producing e^+.

4. Electromagnetic cascade of TeV $\gamma-$rays

As the $\gamma-$rays with an energy ~ 1TeV travel toward the observer, a significant fraction of them will be absorbed due to the interactions with the diffuse infrared background, yielding $e^{\pm}$ pairs [32, 33]. If a primary photon with energy ϵ_γ has been absorbed, the resulting $e^{\pm}$ pairs have Lorentz factors

$$\gamma_e \simeq \epsilon_\gamma/(2m_e c^2) \approx 10^6\ \epsilon_\gamma/(1\,\mathrm{TeV}). \quad (43)$$

Such ultra-relativistic $e^{\pm}$ pairs will subsequently (bulk) Compton scatter on the ambient cosmic microwave background (CMB) photons, and boost them to an average value

$$h\nu_{\rm ic} \sim \gamma_e^2 \bar{\epsilon} \simeq 0.63(1+z)(\epsilon_\gamma/1\,\mathrm{TeV})^2\ \mathrm{GeV}, \quad (44)$$

where $\bar{\epsilon} = 2.7kT_{\rm cmb}$ is the mean energy of the CMB photons with $T_{\rm cmb} \simeq 2.73(1+z)\,\mathrm{K}$.

As shown in [73, 74, 75, 76], there are four timescales involved in the emission process (all are measured by the observer): The first is $t_{\rm act}$, the observed activity time of the source emission. For GRBs, it is unlikely to be longer than 10^3 sec. The second is the well-known angular spreading time

$$\Delta t_{\rm A} \approx (1+z)\frac{R_{\rm pair}}{2\gamma_{\rm e}^2 c} = 960(1+z)(\frac{\gamma_{\rm e}}{10^6})^{-2}(\frac{n_{\rm IR}}{0.1{\rm cm}^{-3}})^{-1}{\rm s},$$

where $R_{\rm pair} = (0.26\sigma_{\rm T} n_{\rm IR})^{-1} \approx 5.8\times10^{25}(\frac{n_{\rm IR}}{0.1{\rm cm}^{-3}})^{-1}{\rm cm}$ is the typical pair-production distance, and $n_{\rm IR} \simeq 0.1{\rm cm}^{-3}$ is the intergalactic infrared photon number density. The third is the inverse Compton cooling timescale

$$\Delta t_{\rm IC} \simeq (1+z)t_{\rm IC,loc}/(2\gamma_e^2) = 38(1+z)^{-3}(\gamma_e/10^6)^{-3}\,{\rm s},$$

where the IC cooling time scale measured in the source frame $t_{\rm IC,loc} = 3m_e c/(4\gamma_e\sigma_T u_{\rm cmb}) = 7.7\times10^{13}(1+z)^{-4}(\gamma_e/10^6)^{-1}\,{\rm s}$, $u_{\rm cmb} = aT_{\rm cmb}^4$ is the CMB energy density, and a is the radiation constant. The fourth is the magnetic deflection time that arises due to the deflection of the pairs by the intergalactic magnetic fields (IGMF):

$$\Delta t_{\rm B} \simeq 6.1\times10^{11}(\frac{\gamma_e}{10^6})^{-5}(\frac{B_{\rm IG}}{10^{-16}{\rm G}})^2(1+z)^{-11}\,{\rm s},$$

where $B_{\rm IG}$ is the strength of the field. Clearly this delay is much too long unless $B_{\rm IG}$ is extremely small.

In the *most optimistic* case, the prompt or very early GRB afterglow fluence in TeV energies would be $\mathcal{S}_{\rm TeV} \sim 10^{-4}$ erg cm^{-2}, thus the expected GeV flux is (assuming $\Delta t_{\rm B}$ dominates $\Delta t_{\rm delay}$)

$$F_{\rm GeV} \approx \frac{\mathcal{S}_{\rm TeV}}{\Delta t_{\rm delay}} \approx 3\times10^{-13}\ (\frac{\gamma_e}{10^6})^5(\frac{B_{\rm IG}}{10^{-16}{\rm G}})^{-2}(\frac{1+z}{2})^{11}(\frac{\mathcal{S}_{\rm TeV}}{10^{-4}{\rm erg\ cm^{-2}}})\ {\rm erg\ cm^{-2}\ s^{-1}}, \quad (45)$$

$B_{\rm IG} \leq 10^{-18}$ G is required to give rise to detectable signals (see also [77, 78]). However, a recent estimate of $B_{\rm IG}$ gives $B_{\rm IG} \sim 10^{-11}$ G [79] and values as large as 0.1μG have been suggested. For such an IGMF, the cascade radiation from the $e^{\pm}$ pairs will appear as a halo around the TeV $\gamma-$ray source because the magnetic field is strong enough to make the distribution of these pairs isotropic [73]. As a result, the flux will be much too low to be detectable.

IV. HIGH ENERGY EMISSION PROCESSES IN GRBS AND AFTERGLOWS

We begin with a brief discussion of the standard theoretical model of GRBs and afterglows (see Fig.6 for a schematic plot) and refer the readers to [7] for a detailed review.

- The bursts are produced by compact sources that generate relativistic outflows — relativistic jets with initial bulk Lorentz factors $\Gamma_o \sim$ tens − hundreds [81, 82, 83].
- The emission is produced by shocks that accelerate particles and generate magnetic fields. An alternative interpretation is that magnetic dissipation via plasma instabilities and reconnection takes place in a Poynting-flux dominated outflow [43, 44, 45]. The shocks (or the magnetic dissipation process) can be internal (if they are within the outflow) [84, 85, 86, 87] or external (if they are due to interaction with the surrounding matter). Note that internal shocks must take place at a radius smaller than the deceleration radius ($\sim 10^{16} - 10^{17}$cm), in which the outflow is slowed down by its interaction with the surrounding matter. Note that also in the case of magnetic dissipation case timing arguments suggest that the dissipation is due to internal processes.
- When the outflow is decelerated by the surrounding medium two distinct shock waves form [88]. A forward shock that expands into the medium,

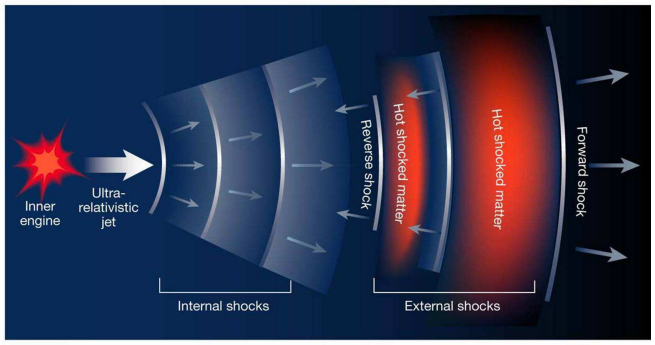

FIG. 6: A schematic plot of internal-external shock model for Gamma-ray Bursts and their afterglows (from [80]).

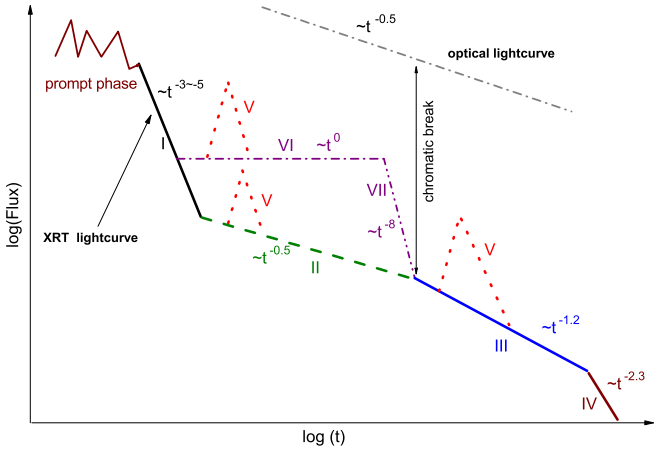

FIG. 7: A schematic plot of the X-ray afterglow of GRBs (see also Zhang et al. [106] and Nousek et al. [107]).

and a reverse shock that penetrates into the outflow. The typical Lorentz factors of the (forward, reverse) shock electrons are $\sim (10^4,\ 10^2)$, respectively. We denote the phase during which both forward and reverse shocks exist as the very early afterglow. In this phase, the forward shock emission peaks in X-ray band while the reverse shock emission peaks in the infrared or optical bands [89]. The reverse shock may lead to an optical flash that begins shortly after the onset of the prompt $\gamma-$ray emission. Such a flash has been detected in several powerful bursts [90, 91]. After the reverse shock crosses the outflow, it dies out and only the forward shock remains. A self similar blast wave forms that propagates into the surrounding material. For a homogenous circumburst medium, the bulk Lorentz factor of the blast wave is [50]

$$\Gamma \approx 6E_{\rm k,53}^{1/8} n^{-1/8} (t/1\ {\rm day})^{-3/8} (1+z)^{3/8}, \qquad (46)$$

where $E_{\rm k}$ is the isotropic-equivalent kinetic energy of the ejecta, and n is the number density of the medium. *Throughout this review, the convention* $G_{\rm x} = G/10^{\rm x}$ *in cgs units has been adopted.* The synchrotron radiation of the shock-accelerated electrons [51, 92, 93] fits the late-time GRB afterglow pretty well [60, 94, 95], though at times jets [96, 97], a wind medium [98, 99, 100], and energy injection [101, 102, 103, 104, 105] had to be invoked to account for the observations.

- Prolonged activity of the GRB central engine also plays an important role in producing afterglow emission (i.e., *the central engine afterglow*) [108, 109] either via late internal shocks [106, 110, 111, 112, 113] or via late magnetic energy dissipation [47, 48, 114]. This activity has been suggested to interpret the peculiar features that emerged in the Swift's observations of the early ($t < 10^4$ sec) X-ray afterglow (see Fig.7): energetic X-ray flares [111, 115, 116], X-ray plateaus that are followed by sharp drops [83, 117] and X-ray flattenings associated with chromatic breaks in the optical band [118, 119, 120].

A. Inverse Compton

Inverse Compton in the form of either SSC [63, 121, 122, 123] or EIC [64, 124, 125] is likely the most important source in producing high energy $\gamma-$ray emission.

1. *Internal shocks SSC*

For internal shocks taking place at a typical radius R, the magnetic field can be estimated as

$$B' \sim [2(1+Y_{\rm ssc})\varepsilon L_{\rm syn}/(\Gamma_o^2 R^2 c)]^{1/2} \sim 10^7\ {\rm Gauss}\ (1+Y_{\rm ssc})^{-1/2} L_{\rm syn,50}^{1/2} \Gamma_o^{-1} R_{13}^{-1}, \qquad (47)$$

where $\varepsilon \equiv \varepsilon_{\rm B}/\varepsilon_{\rm e} \sim (1+Y_{\rm ssc})^{-2}$, and $L_{\rm syn}$ is the synchrotron radiation luminosity of the internal shock emission. The corresponding typical electron Lorentz factor is

$$\gamma'_{e,\rm m} \sim 1400\ (1+Y_{\rm ssc})^{1/4} L_{\rm syn,50}^{-1/4} R_{13}^{1/2} (1+z)^{1/2} (\frac{\epsilon_{\rm p}}{100\ {\rm keV}})^{1/2}, \qquad (48)$$

where $\epsilon_{\rm p} = h\nu_{\rm m}$ is the observed peak energy of the synchrotron emission. The energy of a typical inverse Compton photon is

$$h\nu_{\rm m,ssc} \sim 2\gamma'^2_{e,\rm m}\epsilon_{\rm p} \sim 240{\rm GeV}\ (1+Y_{\rm ssc})^{1/2} L_{\rm syn,50}^{-1/2} R_{13} (1+z) (\frac{\epsilon_{\rm p}}{100\ {\rm keV}})^2. \qquad (49)$$

We summarize the typical values of the parameters involved in eq.(49) and the expected peak energy of the SSC emission in Table III. The SSC spectrum of internal shocks of bright GRBs can show a significant GeV−TeV signal [25, 126], as shown in Fig.8.

TABLE III: SSC emission of internal shocks in the prompt emission phase and in central engine afterglows. $L_{\rm ssc}$ is the SSC radiation luminosity of internal shocks. Note that $L_{\rm ssc}/L_{\rm syn} = Y_{\rm ssc} \sim (-1+\sqrt{1+4\varepsilon_{\rm e}/\varepsilon_{\rm B}})/2 \sim 1$ for $\varepsilon_{\rm e}/\varepsilon_{\rm B} \sim$ a few. In the last column Y, P, N represent Yes, Possible and No respectively.

phases	$L_{\rm syn,50}$	R_{13}	$\epsilon_{\rm p}$/keV	$h\nu_{\rm m,ssc}$	$L_{\rm ssc}/L_{\rm syn}$	Detectability LAT (MAGIC)
GRB	$1-100$	$0.1-10$	10^2-10^3	GeV − TeV	~ 1	Y (P for $z<1$)
X-ray Flash (XRF)	$10^{-3}-1$	$0.1-10$	$\sim$10	GeV	~ 1	Y (N)
Central engine afterglow	$10^{-5}-0.1$	$10-10^2$	$\sim$0.2	sub − GeV	~ 1	P (N)

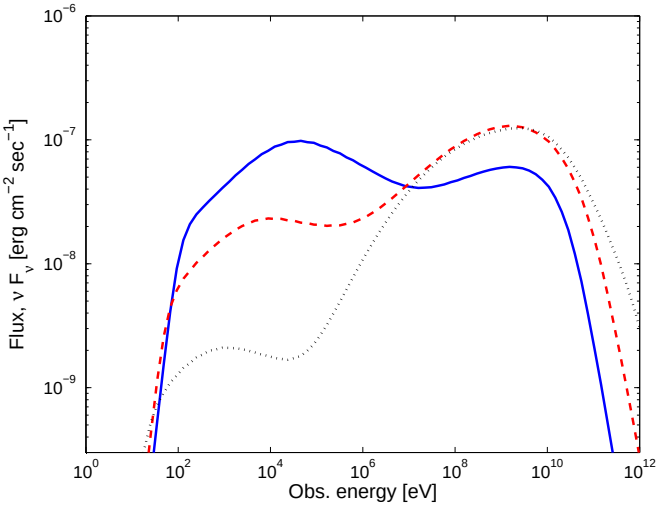

FIG. 8: The GeV excess due to the SSC emission in internal shocks: the synchrotron + SSC spectra of the GRB internal shocks (from [25]). The synchrotron + SSC luminosity $L = 10^{52}$ erg/s, $\varepsilon_{\rm e} = 1/3$, $\Gamma = 600$ and $\delta t_{\rm v} = 10^{-3}$ s for all lines. From top to bottom (i.e., the solid line, the dashed line and the dotted line), $\varepsilon_{\rm B} = (1/3,\ 10^{-2},\ 10^{-4})$, respectively.

Prompt VHE photons above the cut-off frequency $\nu_{\rm cut}$ will produce pairs by interacting with softer photons and will not escape from the fireball. Following [74, 82, 127], we have

$$h\nu_{\rm cut} \approx 2\ {\rm GeV}\ (\epsilon_{\rm p}/100\ {\rm keV})^{(2-p)/p} L_{\rm syn,52}^{-2/p} \delta t_{\rm v,-2}^{2/p} \Gamma_{o,2.5}^{(2p+8)/p}, \quad (50)$$

where $\delta t_{\rm v}$ is the observed variability timescale of the prompt soft $\gamma-$ray emission light curve. Consequently the prompt TeV emission can escape only if $\Gamma_o \geq 10^3$. Additionally, as mentioned in section II B the Universe is optically thick for TeV photons. Hence TeV emission could be detected only for bright (high Γ_o) and nearby GRBs, which of course are quite rare.

For X-ray flashes (XRF) and X-ray rich GRBs, the peak energy is somewhat lower than in GRBs but still above GeV [128]. If the X-ray flare photons are due to the synchrotron radiation of late internal shocks, the SSC emission component will peak at GeV energies and it will be detectable by the upcoming GLAST satellite [24, 125, 129, 131]. If X-ray flares are powered by the refreshed shocks (produced by slowly moving matter that was ejected more or less simultaneously with the faster moving one during the onset of the prompt emission) at a radius $\sim 10^{17}$ cm, the SSC emission may peak in GeV-TeV energy range, as shown in [24, 130]. The X-ray plateaus that are followed by a sharp drop, such those detected in GRB 060607A [83] and GRB 070110 [117], are likely to be the synchrotron radiation of shocks powered by the prolonged activity of the central engine. The SSC radiation components associated with this process appears as GeV plateaus and we expect it to be detectable by LAT [132].

2. *Inverse Compton processes in the very early afterglow*

We denote by *very early afterglow* the short ($\sim 100-1000$ sec) phase during which both forward and reverse shocks exist. This gives a rich structure of possible interactions of photons from different regions with electrons from different regions [123, 134, 135, 136, 137]. The situation is more complicated if the prompt photons overlap the reverse/forward shock fronts. Such an overlap is important if the reverse shock crossing radius satisfies $R_\times \ll 5\times 10^{16}$ cm $\Gamma_{o,2.5}^2 \Delta_{o,11.5}$, where Δ_o is the width of the GRB ejecta [64]. The shock crossing radius $R_\times$ can be written in a general form

$$R_\times \approx \max\{R_\gamma,\ 2\Gamma_\times^2 \Delta_o\}, \quad (51)$$

where R_γ is the radius where the mass of the medium collected by the fireball is equal to $1/\Gamma_o$ of the fireball mass and $\Gamma_\times$ is the Lorentz factor of the shocked ejecta at the crossing time [138]. In eq.(51), the first term dominates if the reverse shock is weak ($\Gamma_\times \sim \Gamma_o/2$), while the second term dominates if the reverse shock is relativistic ($\Gamma_\times \ll \Gamma_o$). Generally we expect that for a weak (relativistic) reverse shock the overlap between the prompt emission and the external shock fronts is unimportant (very important).

Inverse Compton emission can take place in the very early afterglow from either SSC or EIC. There are two cases depending on the strength of the reverse shock. (a) A weak reverse shock, in which the prompt soft $\gamma-$ray photons exceed the external shock fronts quickly. Its effect on cooling the reverse/forward shock electrons is ignorable. In this case, only a factor of ~ 0.1 of the total energy [133] is given to the reverse shock and the rest is given to the forward shock. The seed photons for the

TABLE IV: Inverse Compton emission of very early afterglow

	Rev. shock electrons	For. shock electrons	Cases
Rev. shock photons	$h\nu_{m,\rm ssc}\sim 10\,{\rm keV}(\Gamma/300)^2$	$h\nu_{m,\rm ic}\sim 100\,{\rm MeV}(\Gamma/300)^4$	a, b
For. shock photons	$h\nu_{m,\rm ic}\sim 100\,{\rm MeV}(\Gamma/300)^4$	$h\nu_{m,\rm ssc}\sim 1\,{\rm TeV}(\Gamma/300)^6$	a, b
GRB photons	$h\nu_{m,\rm eic}\sim 1\,{\rm GeV}(\frac{\gamma'_{\rm e,R}}{100})^2(\frac{\epsilon_{\rm p}}{100{\rm keV}})$	Klein-Nishina regime	b
XRF photons	$h\nu_{m,\rm eic}\sim 50\,{\rm MeV}(\frac{\gamma'_{\rm e,R}}{100})^2(\frac{\epsilon_{\rm p}}{5{\rm keV}})$	$h\nu_{m,\rm eic}\sim 5\,{\rm GeV}(\frac{\Gamma}{30})^2(\frac{\epsilon_{\rm p}}{5{\rm keV}})$	b

reverse (forward) shock electrons are their synchrotron radiation and the forward (reverse) shock synchrotron radiation [123, 135]. With typical parameters the energy of the synchrotron photons and the electrons' Lorentz factor in the forward and reverse shocks are [137]:

$$\nu_{\rm syn,F}\sim 10\ {\rm keV}\ (\Gamma/300)^4,\quad \gamma'_{e,\rm F}\sim 10^4(\Gamma/300);$$
$$\nu_{\rm syn,R}\sim 1\ {\rm eV}\ (\Gamma/300)^2,\quad \gamma'_{e,\rm R}\sim 100.$$

As shown in Table IV, there are four inverse Compton processes that produce high energy emission. The most important high energy signature in this case is the GeV−TeV SSC emission of the forward shock.

(b) A strong relativistic reverse shock, for which the overlapping between the prompt emission and the forward/reverse shock regions is tight. In this case, the reverse shock has an energy that is comparable to the forward shock and the prompt emission overlaps the reverse shock front [138]. The reverse shock electrons will be mainly cooled by the prompt ~ 100 keV $\gamma-$rays and give rise to EIC emission with a typical energy [124]

$$h\nu_{m,\rm eic}\sim 2\gamma'^2_{e,\rm R}\epsilon_{\rm p}\sim 1\ {\rm GeV}(\frac{\gamma'_{e,\rm R}}{100})^2(\frac{\epsilon_{\rm p}}{100{\rm keV}}).$$

In the forward shock region, $\gamma'_{e,\rm F}\epsilon_{\rm p}/\Gamma\gg m_{\rm e}c^2$ for $\epsilon_{\rm p}\sim 10^2-10^3$ keV and the EIC process is in the Klein-Nishina regime. So the forward shock electrons will lose their energy mainly via SSC unless the prompt X-ray component is so energetic that can cool the forward shock electrons effectively [64]. If the prompt emission is so soft that $\epsilon_{\rm p}\sim$ a few keV (i.e., XRF) and $\Gamma\sim$ tens, the IC scattering of the forward shock electrons on the prompt emission is still in the Thompson regime and GeV EIC emission is expected. One good candidate is XRF 060218 [139]. The results are summarized in Table IV.

In the case of a dense wind medium, the reverse shock crosses the outflow at a radius $R_\times\sim 10^{15}$ cm $\ll 2\Gamma_o^2\Delta_o$. At such a small radius, because of the tight overlap of the prompt $\gamma-$rays and the forward shock, the optical depth for the GeV−TeV photons produced in the shocks may be very large (see eq.(12) of [64]). These high-energy photons interact with the prompt photons and generate relativistic $e^\pm$ pairs. These pairs re-scatter the soft X-ray photons from the forward shock as well as the prompt photons and power a detectable high-energy emission, a significant part of which is in the sub-GeV energy range. Consequently we will observe an energetic delayed (see eq.(60) below) sub-GeV flash [64].

However, bright optical flashes have been detected only in quite a few bursts (e.g., [90, 91, 140]), for which the afterglow modelling suggests a weakly magnetized ($\sigma\leq 0.1$) reverse shock region ([129, 140, 141, 142, 143], see however [144, 145, 146]). The non-detection of optical flashes in most GRB afterglows may imply a mildly or highly ($\sigma\geq 0.1$) magnetized outflow, in which the SSC emission is very weak. So the contribution of the reverse shock to the high energy emission may be unimportant in most cases (see however [70]).

3. SSC and EIC in the afterglow

During the late afterglow the main radiating region is the forward shock that moves into the surrounding matter. We consider both an ISM ($k=0$) and a wind ($k=2$) medium.

SSC: standard afterglow model. The two characteristic frequencies governing the spectrum are

$$\nu_{m,\rm ssc}\ \approx\ 10^{21}\ {\rm Hz}\ C_p^4\varepsilon_{\rm e,-1}^4\varepsilon_{\rm B,-2}^{1/2}\begin{cases}6.2\ n^{-1/4}E_{\rm k,53}^{\frac{3}{4}}(1+z)^{\frac{5}{4}}t_3^{\frac{-9}{4}}, & \text{for } k=0,\\ 1.4\ A_{*,-1}^{-1/2}E_{\rm k,53}(1+z)t_3^{-2}, & \text{for } k=2,\end{cases}\quad(52)$$

$$\nu_{c,\rm ssc}\ \approx\ 10^{24}\ {\rm Hz}\ (1+Y_{\rm ssc})^{-4}\varepsilon_{\rm B,-2}^{-7/2}\begin{cases}4\ n^{\frac{-9}{4}}E_{\rm k,53}^{\frac{-5}{4}}(1+z)^{\frac{-3}{4}}t_3^{\frac{-1}{4}}, & \text{for } k=0,\\ 1.5\ A_{*,-1}^{\frac{-9}{2}}E_{\rm k,53}(1+z)^{-3}t_3^2, & \text{for } k=2,\end{cases}\quad(53)$$

respectively [63, 68, 122]. Where $C_p\equiv 13(p-2)/[3(p-1)]$, $A_*\equiv[\dot{M}/10^{-5}M_\odot\ {\rm yr}^{-1}][v_w/(10^8{\rm cm\ s}^{-1})]$ is the wind parameter, $\dot{M}$ is the mass loss rate of the progenitor, v_w is the velocity of the wind [100].

The maximum SSC flux can be estimated as [68, 147]

$$F_{\nu,\rm ssc-max}\approx 10^{-11}\ {\rm erg\ cm^{-2}\ s^{-1}\ MeV^{-1}}\begin{cases}0.07\ n^{5/4}\epsilon_{\rm B,-2}^{1/2}E_{\rm k,53}^{5/4}t_3^{1/4}(\frac{1+z}{2})^{3/4}D_{L,28.34}^{-2}, & \text{for } k=0,\\ 1\ A_{*,-1}^{5/2}\epsilon_{\rm B,-2}^{1/2}t_3^{-1}(\frac{1+z}{2})^{2}D_{L,28.34}^{-2}, & \text{for } k=2.\end{cases} \quad (54)$$

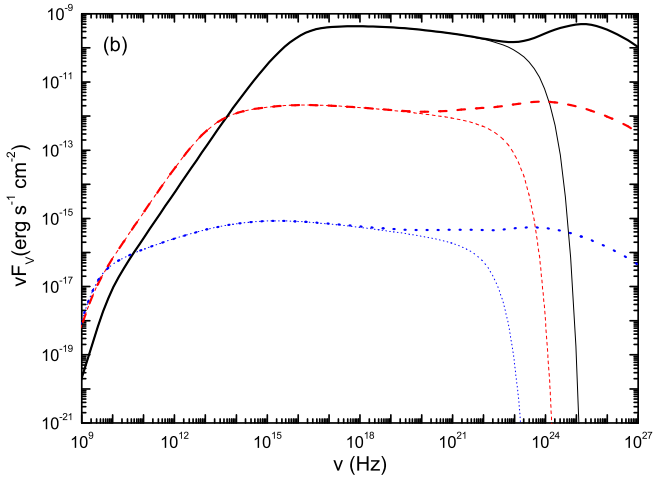

FIG. 9: The multi-wavelength spectra of a GRB forward shock at $2\times(10^2,\ 10^4,\ 10^6)$ sec (from top to bottom). Thin and thick lines correspond to the pure synchrotron spectrum and SSC+synchrotron spectrum, respectively (from [24]). Because of the Klein-Nishina correction, the VHE SSC spectrum is much softer than that of the synchrotron X-rays.

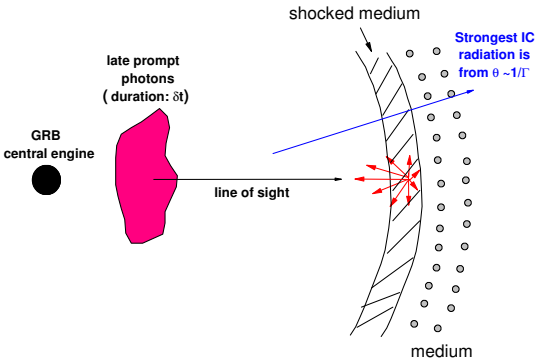

FIG. 10: A schematic plot of the external inverse Compton scattering: the case of the (late) prompt $\gamma-$rays, X-rays and ultraviolet photons from the central engine upscattered by the shock-accelerated electrons in the blast wave (from [152]).

With eqs.(34), we can estimate the SSC emission flux at a given frequency. The relation $\eta=\min\{1,(\nu_m/\nu_c)^{(p-2)/2}\}$ is needed to estimate $Y_{\rm ssc}$, where

$$\frac{\nu_m}{\nu_c}\approx\begin{cases}0.024(1+z)C_p^2\varepsilon_{\rm e,-1}^2\varepsilon_{\rm B,-2}^2nE_{\rm k,53}t_3^{-1}, & \text{for } k=0,\\ 0.12(1+z)^2C_p^2\varepsilon_{\rm e,-1}^2\varepsilon_{\rm B,-2}^2A_{*,-1}^2t_3^{-2}, & \text{for } k=2.\end{cases} \quad (55)$$

A numerical example of the high energy afterglow spectrum is shown in Fig.9.

SSC: modified afterglow model.

The standard GRB fireball model fails to explain the shallow decay phase of the *Swift* GRB X-ray afterglows. As shown in [118, 119, 148, 149], we need to consider various modifications: (1) The fireball undergoes a significant energy injection, i.e., $E_{\rm k}\propto t^{1-q}$ [104, 105]; (2) The shock parameters are shock-strength dependent [118, 148], i.e., $\varepsilon_{\rm e}\propto\Gamma^{-a}$ and $\varepsilon_{\rm B}\propto\Gamma^{-b}$. In both cases, an early flattening is expected in the high energy afterglow light curve, as shown in [24, 130, 147, 150, 151]. Without these modifications, both $E_{\rm k}$ and $\varepsilon_{\rm e}$ take a constant value from the beginning. The early time X-ray emission would be stronger but drop with time faster. The weak X-ray signal in the early afterglow phase implies a less optimistic detection prospect of the GeV emission [14, 24, 150] (see however [151]).

Table V gives the spectral and temporal indexes α and β of the afterglow emission. We define $\alpha=\alpha_0+\alpha_E+\alpha_v+\alpha_Y$, where α_0 corresponds to the contribution of the standard emission, α_E represents the contribution of the energy injection, α_v stands for the contribution of evolving shock parameters, and α_Y comes from the evolution of Compton parameter $Y_{\rm ssc}$. For example, if we only consider energy injection, then $\alpha=\alpha_0+\alpha_E$. If only evolving shock parameters is considered, $\alpha=\alpha_0+\alpha_v$. If both effects are considered, $\alpha=\alpha_0+\alpha_E+\alpha_v$. If $Y_{\rm ssc}\gg1$, the term α_Y should be included [147].

EIC. It has been suggested that some GRB central engines produce late prompt emission in the form of X-ray flares or X-ray plateaus followed by sharp drops. These late prompt photons with an energy $\epsilon_{\rm x}$ will catch up with the blast wave, cool the shock-accelerated electrons and give rise to EIC emission [125, 152], as shown in Fig.10. In this case, the peak energy of the EIC emission is

$$h\nu_{m,\rm eic}\sim 0.4\ {\rm GeV}\ \gamma'^2_{m,3}(\epsilon_{\rm x}/0.2{\rm keV}), \quad (56)$$

where

$$\gamma'_m\ \sim\ 1.7\times10^3\ \varepsilon_{\rm e,-1}C_p \begin{cases}E_{\rm k,53}^{1/8}n_0^{-1/8}t_3^{-3/8}[(1+z)/2]^{3/8}, & \text{for } k=0,\\ E_{\rm k,53}^{1/4}A_{*,-1}^{-1/4}t_3^{-1/4}[(1+z)/2]^{1/4}, & \text{for } k=2.\end{cases} \quad (57)$$

A novel phenomena that appears in the EIC process is that the duration of the high energy emission is significantly longer than the duration of the seed photon pulse.

TABLE V: The spectral and temporal index β, α of afterglow emission in the case of ISM. Here $F_\nu \propto \nu^{-\beta} t^{-\alpha}$ is adopted (from [147]).

	β	α_0	α_E	α_v	α_Y
Synchrotron				Slow Cooling	
$\nu < \nu_m$	$-\frac{1}{3}$	$-\frac{1}{2}$	$-\frac{5(1-q)}{6}$	$\frac{2a-b}{8}$	0
$\nu_m < \nu < \nu_c$	$\frac{p-1}{2}$	$\frac{3(p-1)}{4}$	$-\frac{(1-q)(p+3)}{4}$	$-\frac{12a(p-1)+3b(p+1)}{32}$	0
$\nu_c < \nu$	$\frac{p}{2}$	$\frac{3p-2}{4}$	$-\frac{(1-q)(p+2)}{4}$	$-\frac{12a(p-1)+3b(p-2)}{32}$	$-\frac{4q(p-2)-3a(p-1)-3b(p-3)}{8(4-p)}$
Synchrotron				Fast Cooling	
$\nu < \nu_c$	$-\frac{1}{3}$	$-\frac{1}{6}$	$-\frac{7(1-q)}{6}$	$-\frac{3b}{8}$	$-\frac{a-b}{8}$
$\nu_c < \nu < \nu_m$	$\frac{1}{2}$	$\frac{1}{4}$	$-\frac{3(1-q)}{4}$	$\frac{3b}{32}$	$\frac{3(a-b)}{16}$
$\nu_m < \nu$	$\frac{p}{2}$	$\frac{3p-2}{4}$	$-\frac{(1-q)(p+2)}{4}$	$-\frac{12a(p-1)+3b(p-2)}{32}$	$\frac{3(a-b)}{16}$
SSC				Slow Cooling	
$\nu < \nu_{m,\rm ssc}$	$-\frac{1}{3}$	-1	$-(1-q)$	$\frac{4a-b}{8}$	0
$\nu_{m,\rm ssc} < \nu < \nu_{c,\rm ssc}$	$\frac{p-1}{2}$	$\frac{9p-11}{8}$	$-\frac{(1-q)(3p+7)}{8}$	$-\frac{24a(p-1)+3b(p+1)}{32}$	0
$\nu_{c,\rm ssc} < \nu$	$\frac{p}{2}$	$\frac{9p-10}{8}$	$-\frac{(1-q)(3p+2)}{8}$	$-\frac{24a(p-1)-3b(6-p)}{32}$	$-\frac{4q(p-2)-3a(p-1)-3b(p-3)}{4(4-p)}$
SSC				Fast Cooling	
$\nu < \nu_{c,\rm ssc}$	$-\frac{1}{3}$	$-\frac{1}{3}$	$-\frac{5(1-q)}{3}$	$-\frac{5b}{8}$	$-\frac{(a-b)}{4}$
$\nu_{c,\rm ssc} < \nu < \nu_{m,\rm ssc}$	$\frac{1}{2}$	$-\frac{1}{8}$	$-\frac{5(1-q)}{8}$	$\frac{15b}{32}$	$\frac{3(a-b)}{8}$
$\nu_{m,\rm ssc} < \nu$	$\frac{p}{2}$	$\frac{9p-10}{8}$	$-\frac{(1-q)(3p+2)}{8}$	$-\frac{24a(p-1)-3b(6-p)}{32}$	$\frac{3(a-b)}{8}$

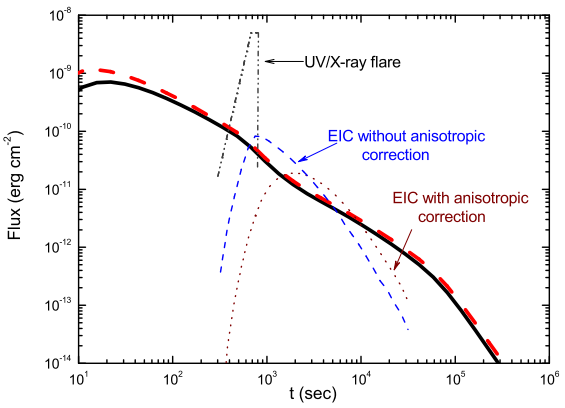

FIG. 11: The EIC emission with (the dotted line) and without (the thin dashed line) anisotropic correction (from [24]). The thick lines are the SSC emission of the forward shock in two different energy ranges.

This is because the duration of the high energy emission is affected by the spherical curvature of the blast wave [124] and is further extended by the highly anisotropic radiation of the up-scattered photons [152]. One can see these two effects, particularly the second one, in Fig.11. Below, following [24], we give an analytical derivation of the peak time of the EIC emission caused by a seed photon pulse. For electrons with an energy distribution $dn'/d\gamma'_e \propto {\gamma'_e}^{-p}$, if the IC scattering is in Thompson regime (i.e., $\xi \ll 1$), with eq.(37) we can show that in the local frame of the shocked medium, the resulting EIC emissivity is proportional to $(1-\cos\theta_{\rm sc})^{(1+p)/2}$ [72]. The observed emission from an angle θ is thus

$$\begin{aligned} \mathcal{F} &\propto \mathcal{D}^3 \sin\theta (1-\cos\theta_{\rm sc})^{(1+p)/2} \\ &\propto \theta^{p+2}(1+\Gamma^2\theta^2)^{-(7+p)/2}. \end{aligned} \tag{58}$$

The term $\mathcal{D}^3$ is caused by Lorentz translation of the emitting power, $\sin\theta$ is from the expression of the solid angle, and $(1-\cos\theta_{\rm sc})^{(1+p)/2}$ is the anisotropic correction of the EIC.

We define a θ_c at which the emission peaks (i.e., $\frac{d\mathcal{F}}{d\theta}\,|_{\theta=\theta_c} = 0$) and have

$$\theta_c \approx (\frac{2+p}{5})^{1/2}\Gamma^{-1} \approx 1/\Gamma. \tag{59}$$

The EIC emission thus *peaks* at a time

$$T_p \approx (1+z)R(1-\cos\theta_c)/c \approx \frac{(1+z)R}{2\Gamma^2 c}, \tag{60}$$

where R is the radius of the shock front.

For UV/X-ray flares having a duration $\delta t \sim 0.3 t_{\rm f}$, the duration of the EIC emission is $T_{\rm eic} \sim T_p \sim 3t_{\rm f}$, where $t_{\rm f}$ is the flare peak time. As a result, $T_{\rm eic} \sim 10\delta t$.

The luminosity of the EIC emission can thus be estimated as

$$L_{\rm eic} \approx \frac{L_{\rm eln}(t_{\rm f})\delta t}{T_{\rm eic}} \approx \frac{L_{\rm eln}(t_{\rm f})\delta t}{T_p} \ll L_{\rm eln}(t_{\rm f}), \tag{61}$$

where $L_{\rm eln}$ is the power given to the freshly shocked electrons in the blast wave and can be estimated as

$$\begin{aligned} L_{\rm eln} &\sim \varepsilon_{\rm e,-1} E_{\rm k,53}(1+z)t_3^{-1} \\ &\begin{cases} 7.5\times10^{48}\ {\rm erg\ s^{-1}}, & \text{for } k=0, \\ 5\times10^{48}\ {\rm erg\ s^{-1}}, & \text{for } k=2. \end{cases} \end{aligned} \tag{62}$$

We note that $L_{\rm eln}$ depends only weakly on the density profile.

4. Bulk Compton

Shemi [153] and Shaviv & Dar [154, 155] proposed bulk Compton scattering as the source of the prompt $\gamma-$ray emission. In their scenario, the ultra-relativistic ejecta is moving into a dense soft photon background and the electrons in the ejecta Compton scatter on these photons and boost them to MeV energies (see also [156]).

Bulk Compton scattering can also take place in internal shocks, as suggested by Takagi & Kobayashi [157]. In this case, the seed photons are the synchrotron photons emitted by one of the internal shocks. They are up-scattered by the electrons carried by faster shell(s) ejected at late times (before this shell collides so the electrons are cold). The bulk Compton scattering produces a 100MeV-GeV emission component if the sub-outflows' Lorentz factor varies significantly, say, between 10 and 10^4. The efficiency of producing high energy emission in such a process, however, is low to $\sim 0.001 - 0.01$ for baryon-rich outflows.

Recently, Panaitescu [158] suggested that the X-ray flares, the X-ray plateau followed by a sharp drop, and the shallow decay X-ray phase that ends without an optical break are produced by bulk Compton scattering of the forward shock synchrotron photons by electrons carried in a new outflow launched by the central engine. In this model, the bulk Lorentz factor of the new outflow $\Gamma_{\rm new}$ has to be much larger than the decelerating GRB outflow. In [158], $\Gamma_{\rm new}$ is taken to be $\sim 10^4 - 10^5$. The new outflow has also to be $e^{\pm}$ pairs dominated otherwise the efficiency of energy conversion in the bulk Compton scattering process would be very low [157]. It is not clear whether these two conditions are realistic or not. If correct, a GeV emission component associated with the peculiar X-ray afterglow should be present [159]. Unfortunately, it is difficult to distinguish this scenario from the regular model discussed earlier because of the small differences in temporal/spectral behaviors of the GeV emission.

B. Other high energy processes in GRBs and afterglows

1. High energy $\gamma-$rays from pion production

Katz [160] introduced pion production to explain the delayed 18 GeV photons of GRB 940217. In his model, these energetic photons resulted from collisions of relativistic nucleons with $\Gamma \sim 300$ with a dense surrounding cloud, producing π^0, and decaying to tens GeV photons [160].

The GRB outflow might be neutron-rich [161]. In a neutron-rich fireball, if the initial entropy > 400, the neutrons and protons acquire a relative drift velocity causing inelastic n, p collisions and creating π^0 and yielding ~ 10 GeV photons [162, 163].

In GRB internal shocks, protons can be accelerated to very high energies and photonpion collision create π^0 or Δ^+ which in turn produces high energy photons. These photons are so energetic that they can not escape from the fireball (see eq.(50)) [26]. Dermer & Atoyan [164] argued that the ultra-high energy neutrons created in the $p + \gamma$ process play a crucial role in producing GeV emission. These neutrons are not confined by the magnetic field of the blast-wave shell and flow out, and are subject to further photo-pion processes with photons in the surrounding medium to form charged and neutral pions. The charged pions decay into ultra-relativistic electrons and neutrinos, whereas the decay of π^0 produces two $\gamma-$rays that are promptly converted into electron-positron pairs on the assumed Gauss-strength magnetic fields surrounding GRB sources. The synchrotron radiation of these energetic pairs can give rise to a strong GeV emission and may be able to account for the hard $\gamma-$ray component detected in GRB 941017 [164]. Ioka et al. [165] considered the β-decay of the ultra-relativistic neutral beam ($n \rightarrow p + e^- + \bar{\nu}_e$) and predicted extended GeV-TeV emission surrounding Gamma-Ray Burst remnants.

2. Electromagnetic cascade of TeV $\gamma-$ rays

The electromagnetic cascade of TeV $\gamma-$rays was introduced by Plaga [73] as a model for the long-lasting MeV-GeV afterglow emission of GRB 940217 (see also [166]). In this model TeV emission from the bursts cascade on the CMBR. Dai & Lu [74] and Wang et al. [167] proposed that the SSC emission of internal shocks (see also [128, 168]) or the very early forward shock may peak at TeV energies and then calculated the delayed MeV-GeV emission resulting in the electromagnetic cascade. Detailed modeling of the electromagnetic cascade of GRB TeV emission has been carried out in [77, 78]. However this model requires a very low IGM field $< 10^{-18}$ G, otherwise the resulting emission will be extremely weak (see eq.(45)).

V. INTERPRETATIONS OF CURRENT OBSERVATIONS

So far there are only few high energy GRB observations and in most cases the data is insufficient to carry out a detailed analysis. Most cases are consistent with SSC or EIC interpretation either from the prompt emission or from the afterglow shocks or from both. However, numerous other models have been put forwards.

- González et al. [23] discovered a significant sub-GeV emission in 26 bright GRBs (including GRB 941017) during the prompt phase. In these cases the high energy spectra are consistent with the single power law component observed by BATSE. The simplest and the most natural interpretation

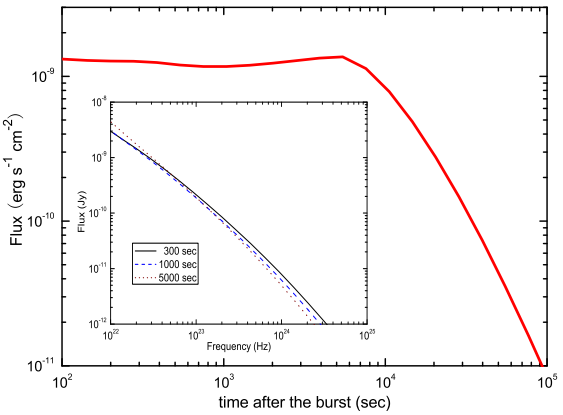

FIG. 12: The SSC radiation of the forward shock undergoing energy injection and with evolving shock parameters, the case of GRB 940217: the thick solid line is the light curve and the inserted plot is the spectrum (the times have been marked in the plot), in the energy range of 30 MeV - 30 GeV (from [147]).

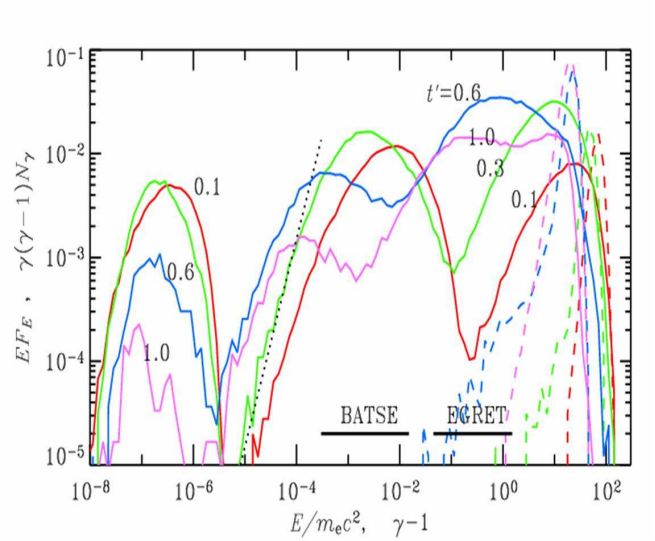

FIG. 13: The SSC and the second order inverse Compton emission of internal shocks that have a synchrotron radiation peaking in UV/optical band (from [69]). Note that in this figure the photons' energy, in units of m_ec^2, is measured in the rest frame of the GRB ejecta and not in the observer's frame.

of the prompt high energy $\gamma-$rays is an internal shock synchrotron radiation in the MeV-GeV energy range. Similar conclusion can be drawn for the GeV excesses seen in GRB 920622 and GRB 940301 [18].

- The discovery of a 18 GeV photon about one hour after GRB 940217 is very amazing. The other 17 high energy photons detected in phase-2 have similar energy $\simeq$ 100 MeV (see Fig.3). Excluding the 18 GeV photon, the count rate and the energy of the high energy photons are almost constant.

  A slowly decaying MeV$-$GeV afterglow light curve is possible in the standard afterglow shock model if $\nu_{c,\rm ssc} < \nu < \nu_{m,\rm ssc}$ (see Table V). This interpretation, however, suggests $\beta \sim 1/2$, which is inconsistent with the observation $\beta \sim 1.8$ and thus is *unlikely*. Wei & Fan [147] suggest that the SSC of a modified forward shock can reproduce the data. Their numerical results are shown in Fig.12. An alternative is that the MeV-GeV plateau was the SSC radiation component of an X-ray plateau like that detected in GRB 070110. The two models differ in the origin of the seed photons. In one case it is the forward shock X-ray emission and in the other a central engine afterglow.

- In GRB 941017, both the duration and the fluence of the high energy emission component are about 3 times that of prompt soft $\gamma-$rays. The spectrum of these hard gamma-rays is unusually hard ($F_\nu \propto \nu^0$).

  Granot & Guetta [135] (see also [137]) suggested that inverse Compton from reverse shock is most likely to provide the right temporal behavior. Because of the very large energy emitted in hard $\gamma-$rays, the reverse shock has to be relativistic. The second possibility is the inverse Compton from very early forward shock while the reverse shock is still going on. In both cases, the prompt soft $\gamma-$rays overlap the shocked regions (as seen in the data, it is indeed the case), and plays an important role by providing the seed photons for an EIC process that gives rise to the strong GeV emission [64, 124]. Two additional advantages of the EIC model are: (a) As shown in eq.(60) and in Fig.11, the duration of the high energy emission is naturally much longer than that of the seed photons (here the prompt soft $\gamma-$ray emission); (b) The spectrum could be as hard as $F_\nu \propto \nu^{-1/2\sim 1/3}$, as shown in figure 13 of [24].

  Dermer & Atoyan [164] proposed a neutral beam model (see section IV B 1) to explain the very hard spectrum $F_\nu \propto \nu^0$, in which a Gauss-strength magnetic fields of the circumburst medium is needed.

- Although no very high energy emission was directly detected from GRB 080319B the unique prompt spectrum of this bursts suggests that it has been accompanied by a very strong GeV emission that would have carried at least 10 times more energy in the GeV component than in the prompt MeV emission (see [169] for details).

  GRB 080319B was located at redshift $z = 0.937$. The peak energy of the spectrum was $E_{\rm p} \sim 600$

keV, and the photon indexes below and above $E_{\rm p}$ are ~ -0.8 and ~ -3.4 respectively [170]. The peak prompt V-band ($\nu_{\rm v} \sim 5\times10^{14}$ Hz) emission reached $\sim$ 5th magnitude [170]. The spectrum of the optical to soft $\gamma-$ray emission cannot be interpreted as a simple synchrotron spectrum as the low energy optical component is much too large.

A possible solution is that the UV/optical emission is the synchrotron radiation of the internal shocks while the soft $\gamma-$rays are the corresponding SSC emission, i.e, $h\nu_m \sim 10$ eV and $h\nu_{m,\rm ssc} \sim E_{\rm p} \sim 600$ keV. So the typical Lorentz factor of the emitting electrons is $\gamma'_{e,\rm m} \sim (\nu_{m,\rm ssc}/\nu_m)^{1/2} \sim 200$. The unusual spectrum of the $\gamma-$rays suggests a cooling Lorentz factor $\gamma'_{e,c} \sim \gamma'_{e,\rm m}$. On the other hand, $\gamma'_{e,c} \sim 500\ \Gamma^3_{o,3}R_{16}L^{-1}_{\rm syn,52}[\varepsilon(1+Y_{\rm 2ndIC})^2]^{-1}$. To derive this relation, the term $(1+Y_{\rm ssc})$ of eq.(47) should be replaced by $(1+Y_{\rm 2ndIC})$ because in this particular burst the 2nd-order IC is very important, as shown below. Given the observation $h\nu_{\rm v}F_{\nu_{\rm v}}/E_{\rm p}F_{E_{\rm p}} \sim 1/100$ and given that $F_\nu \propto \nu^{1/3}$ at energies $< h\nu_m$, we have $Y_{\rm ssc} \sim 100/(\nu_m/\nu_{\rm v})^{4/3} \sim 10$. Note that these estimates are not very sensitive to the choice of the (unknown) value of ν_m. Correspondingly $\varepsilon = \varepsilon_{\rm B}/\varepsilon_{\rm e} \sim Y^{-3/2}_{\rm 2ndIC} \sim Y^{-3}_{\rm ssc} \sim 0.001$ (which suggests, incidentally, that the outflow is not Poynting-flux dominated). A $\gamma'_{e,\rm c} \sim 200$ thus requires that $(\Gamma_o,\ R) \sim (10^3,\ 10^{16}$ cm). The 2nd-order IC scattering of the internal shock electrons is still in the Thompson regime since $\gamma'_{e,\rm m}E_{\rm p}/\Gamma_o < m_{\rm e}c^2$. The spectrum peaks at $\sim 2\gamma'^2_{e,\rm m}E_{\rm p} \sim 40$ GeV and can escape the fireball freely. The luminosity of the 2nd order IC emission may be as high as $\sim 10^{53}$ erg s^{-1}. According to this model a significant GeV emission might have been detected by AGILE if it was not occulted by Earth at that moment [169]. It is very interesting to note that such a scenario has been outlined by Stern & Poutanen [69], as shown in Fig.13.

Two additional high energy components with a duration $\sim$ 100 s (i.e., longer than duration of the prompt 2nd-order IC emission) could arise in this burst. The optical emission in the time range of $100-1000$ sec is probably the high latitude emission of the reverse shock [170]. This interpretation implies that the reverse shock was relativistic and there was an overlap between the prompt emission and the reverse shock region. In this case, the reverse shock electrons would be effectively cooled by the prompt photons (see section IV A 2) and would give rise to GeV-TeV EIC emission with a luminosity $\sim 10^{52}$ erg s^{-1}. The huge amount of prompt UV/optical photons would cool the forward shock electrons effectively and give rise to another GeV-TeV EIC emission with a luminosity $\sim 10^{52}$ erg s^{-1} (see [169]).

VI. SUMMARY AND OUTLOOK

We have reviewed the observation of the prompt and afterglow high energy emission from GRBs (Sec. II), then concentrated on the possible physical processes giving rise to these signals (Sec. III) and applied them to GRBs and their afterglows (Sec. IV). The likely interpretations of the observations have been presented in Sec. V.

After reviewing various possible sources for very high energy emission we find, somewhat expectedly, that the most important source for very high energy emission in GRBs and their afterglows is inverse Compton either in the form of SSC or EIC. Our discussion has been based on the standard baryon-rich fireball model, which works pretty well in modeling late time GRB afterglow data (see [8, 11, 14] for reviews).

The high energy emission is expected to be strong in the prompt emission phase and the early afterglow. The current limited data can be interpreted within the framework of the fireball model, though at times some modifications are needed. Future high energy observation, particularly in the early afterglow phase, will impose tighter constraint on these modifications.

We expect that the internal shock SSC emission in both prompt emission phase and in central engine afterglows will be detectable by LAT in the MeV-GeV energy range (see Table III). The higher than 50GeV SSC emission from internal shocks is expected to be detectable only for some extremely bright GRBs with a $\Gamma_o \geq 10^3$ and a $z < 1$. A rough estimate of the detectable count rates of high energy photons from GRB forward shock by LAT and MAGIC is summarized in Table VI. Recently Xue et al. [171] calculated the VHE SSC emission of the forward shock of specific nearby GRBs having a $z < 0.25$ and found that a significant detection was expected only in GRB 030329. The results are consistent with the null detection of MAGIC [29], Whipple [41] and H.E.S.S. [42]. MAGIC-II and H.E.S.S.-II will lower the energy threshold to about 30 GeV. With a very large effective area $\sim (1-5)\times10^7$ cm^2 and the much less absorption by the IR-background, significant detections of the tens GeV photons from GRBs and afterglows will be possible. We may be able to use these detections to calibrate the IBL models at high redshifts. Below we focus on the MeV-GeV signatures that are detectable by LAT and the possible constraints on the astrophysical model that might arise from this new data. We divide this discussion to the prompt emission and the afterglow:

Prompt Emission

The field of view of GBM is all sky not occulted by the earth and that of LAT is $\sim$ 2.5 sr. So $\sim 1/5$ GRBs will be within the field of view of both GBM and LAT. With a good quality keV$-$GeV spectrum, we may achieve the following goals:

- The particle acceleration process in GRBs can be better constrained. In principle, the electrons can

TABLE VI: Expected signals from GRB forward shock SSC emission. The absorption of the VHE photons by infrared background has been taken into account, based on Table II. These values are calculated for a typical burst with $E_{\rm k}\sim 10^{53}$erg (at the end of the X-ray shallow decline) and $z=1$, correspondingly to the burst with a sub-MeV $\gamma-$ray fluence of $\sim 10^{-5}$ erg cm^{-2} (from [24]). Note that we have used for Magic an effective area, in the energy range of 50GeV-10TeV, of $S_{\rm det}\sim 10^5$ m^2. This might be an overestimate for ~ 50 GeV.

	$N_{\rm det}(>20{\rm MeV})$ LAT	$N_{\rm det}(>10{\rm GeV})$ LAT (1m^2)	$N_{\rm det}(>50{\rm GeV})$ MAGIC (10^5m^2)
Standard afterglow: ISM	~ 13	$\sim 10\times 10^{-2}$	~ 11
Standard afterglow: wind	~ 12	$\sim 8\times 10^{-2}$	~ 7
Energy injection: ISM	~ 3	$\sim 2\times 10^{-2}$	~ 2
Energy injection: wind	~ 4	$\sim 2\times 10^{-2}$	~ 2
Time increasing $\varepsilon_{\rm e}$: ISM	~ 3	$\sim 2\times 10^{-2}$	~ 2
Time increasing $\varepsilon_{\rm e}$: wind	~ 3	$\sim 1\times 10^{-2}$	~ 1

be accelerated to an energy $\sim 20B'^{-1/2}$ TeV (measured in the rest frame of the emitting region) and can give rise to GeV synchrotron radiation (see eq.(16)). A cut-off at much lower energy (say, a few MeV) will challenge the internal shock model or the currently adopted particle acceleration model, that assumes $dn'/d\gamma'_e\propto\gamma'^{-p}_e$.

- The escape of the most energetic prompt photons from the fireball depends strongly on Γ_o the bulk Lorentz factor of the GRB ejecta (see eq.(50)) [82] and on the radius of the internal energy dissipation [172]. A detected GeV cutoff would constrain these two parameters (unless the redshift is sufficiently large that the cosmological attenuation will give rise to such a cutoff too (see Fig.2)).

- A strong SSC GeV emission component is expected in the standard baryonic dominated model. A lack of such emission in the prompt spectrum may favor the internal magnetic energy dissipation model for the prompt $\gamma-$rays [43, 44, 46], in which the inverse Compton effect is weak (unless Γ_o or $\delta t_{\rm v}$ is very small (see eq.(50)).

Actually, as shown in the last paragraph of section V, the prompt GeV emission of GRB 080319B may have a luminosity as large as $\sim 10^{53}$ erg s^{-1} or even larger, which is ~ 10 times more energetic than the prompt optical$-$MeV emission. AGILE GRID should have detected such an amazing component if it was not occulted by the earth at that moment. Such a detection would be crucial to pin down the prompt emission mechanism(s).

Afterglow

The afterglow, and in particular the early afterglow is an additional powerful source of very high energy emission. Motivated by the identification of a canonical X-ray afterglow light curve of *Swift* GRBs [106, 107], Fan et al. [24] argued that a similar high energy emission light curve should be observed (Fig.14). Given the small number of expected high energy photons (typically ~ 10 for a bright burst at redshift $z\sim 1$) detectable for LAT, these novel features are not likely to be identified as frequently as in X-ray band. However, a detection of more than 10^2-10^3 sub$-$GeV photons is possible in some extremely bright bursts and these case can be used to test the prediction shown in Fig.14.

- EGRET had discovered long-lasting MeV-GeV plateau in GRB 940217 and an energetic delayed sub-GeV plateau in GRB 941017. These are good candidates of a *shallow decline (or plateau) phase* and very early *EIC plateau* of the high energy afterglow light curve shown in Fig.14. LAT is expected to detect more such cases in the coming years.

- The SSC emission of central engine afterglows, such as X-ray flares and X-ray plateaus followed by a sharp drop, may give rise to detectable sub-GeV flares and plateaus. The EIC emission component usually lasts much longer than the seed photon pulse and may be outshined by the SSC emission component of the forward shock (see Fig.11). As long as $Y_{\rm ssc}\geq 1$ and the forward shock electrons are in fast cooling, the EIC process can not enhance the detectability of the high energy afterglow a lot because in the absence of EIC, the SSC will radiate significant part of the energy $L_{\rm eln}$ into GeV energies. Distinguished EIC signatures are expected if the forward shock cools very inefficiently before the flare.

- The establishment of a canonical high energy afterglow light curve in some extremely bright GRBs will confirm current interpretations of the peculiar *Swift* X-ray afterglow data.

The prospects for these advanced are good. The very high emission might provide essential clues to the nature of GRBs and in particular to the elusive conditions within the emitting regions and the emission processes. However, as suggested by past experience new challenges and surprises are bound to emerge when a new observational window is opened and new observations become available. GLAST LAT, on one hand and new improved Cenrenkov telescopes, with a larger collection area and

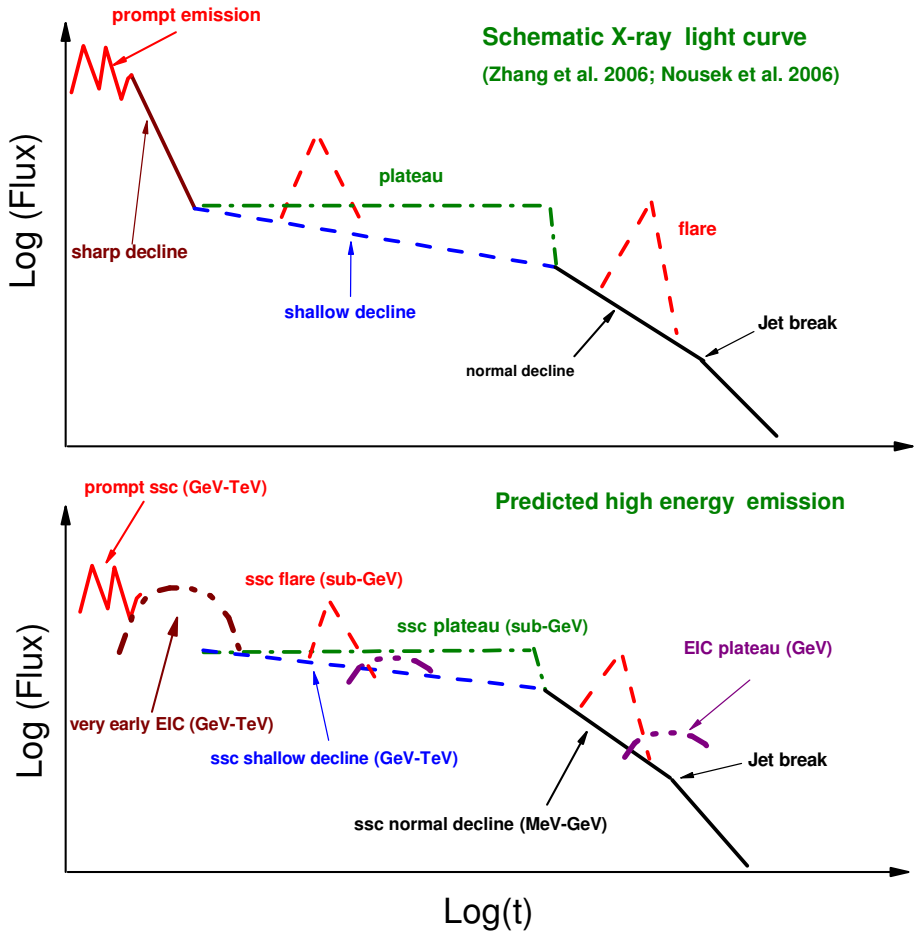

FIG. 14: The expected high energy emission signatures are shown in the lower panel, corresponding to the schematic X-ray light curve shown in the upper panel (from [24]). Please note that the SSC flares could be in GeV-TeV energy range if the X-ray flares are powered by external shocks.

a lower energy detection threshold, on the other, may provide such surprises in the near future.

Acknowledgments

We thank T. Lu, S. Covino, Z. G. Dai, B. Zhang, D. M. Wei, P. H. Tam, K. Murase, X. F. Wu and Y. C. Zou for comments and/or communications. This work is supported by a (postdoctoral) grant from the Danish National Science Foundation, the National Science Foundation (grant 10673034) of China, a special grant of Chinese Academy of Sciences (Y.Z.F), and US-Israel BSF (T.P). TP acknowledges the support of Schwartzmann University Chair.

[1] Klebesadel R. W., Strong I. B., and Olson R. A., Astrophys. J., 1973, 182: L85
[2] Fishman G. J. and Meegan C. A., Annu. Rev. Astron. Astrophys, 1995, 33: 415
[3] Metzger M. R., et al., 1997, Nature, 387, 878
[4] Costa E., et al., Nature, 1997, 387: 783
[5] van Paradijs J., et al., Nature, 1997, 386: 686
[6] Frail D., et al., Nature, 1997, 389: 261
[7] Piran T., Phys. Rep., 1999, 314: 575
[8] Piran T., Rev. Mod. Phys., 2004, 76: 1143
[9] Cheng K. S. and Lu T., Chin. J. Astron. Astrophys., 2001, 1: 1

[10] Mészáros P., Annu. Rev. Astron. Astrophys, 2002, 40: 137
[11] Mészáros P., Rep. Prog. Phys., 2006, 69: 2259
[12] Lu T., Huang Y.F., Dai Z.G., and Wei D.M. Gamma-Ray Bursts,invited talk presented at the International Conference on the Multiwavelength Approach to Unidentified Gamma-Ray Sources, published as the Chapter 10 of the book COSMIC GAMMA-RAY SOURCES(ed. K.S. Cheng & G.E. Romero), Hong Kong, Kluwer Academic Publishers, 2004, 225-260
[13] Zhang B. and Mészáros P. Int. J. Mod. Phys. A, 2004, 19: 2385
[14] Zhang B., Chin. J. Astron. Astrophys., 2007, 7: 1
[15] Nakar E., Phys. Rep., 2007, 442: 166
[16] Lee W. H. and Ramirez-Ruiz E. 2007, New. J. Phys., 9: 17
[17] Schneid E. J., et al., Astron. Astrophys., 1992, 255: L13
[18] Schneid E. J., et al., Astrophys. J., 1995, 453: 95
[19] Dingus B. L., Astrophys. Spa. Sci., 1995, 231: 187
[20] Sommer M., et al., Astrophys. J., 1994, 422: L63
[21] Hurley K., et al., Nature, 1994, 372: 652
[22] Schaefer B. E., et al., Astrophys. J., 1998, 492: 696
[23] González M. M., et al., Nature, 2003, 424: 749
[24] Fan Y. Z., Piran T., Rarayan R., and Wei D. M., 2008, Mon. Not. R. Astron. Soc., 384: 1483
[25] Pe'er A. and Waxman E., Astrophys. J., 2004, 613: 448
[26] Gupta N. and Zhang B., Mon. Not. R. Astron. Soc., 2007, 380: 78
[27] Pittori C., Chin. J. Astron. Astrophys. Supplement., 2003, 3: 517
[28] Saz Parkinson P. M. and Dingus B. L., 2007 (arXiv:0710.2350)
[29] Albert J., et al., Astrophys. J., 2007, 667: 358
[30] Aharonian F., et al., Astron. Astrophys., 2006, 457: 899
[31] Holder J., et al., Astropart. Phys., 2006, 25: 391
[32] Nikoshov A. I., Sov. Phys.-JETP, 1962, 14: 393
[33] Gould R. J. and Schréder G. P., Phys. Rev., 1967, 155: 1408
[34] Stecker F. W., Malkan, M. A., Scully S. T., Astrophys. J., 2006, 648: 774
[35] Stecker F. W., Malkan, M. A., Scully S. T., Astrophys. J., 2007, 658: 1392
[36] Aharonian F., et al., Nature, 2006, 440: 1018
[37] Hartmann D. H., AIP Conf. Proc., 2007, 921: 24
[38] Dermer C. D. and Chiang J., AIP Conf. Proc., 2000, 515: 225
[39] Atkins R., et al., Astrophys. J., 2000, 533: L119
[40] Bastieri D., et al., ICRC, 2007 (arXiv:0709.1380)
[41] Horan D., et al., Astrophys. J., 2007, 655: 396
[42] Tam P. H., et al., submitted to ICRC, 2007 (arXiv:0710.4057, p.157)
[43] Usov V. V., 1994, Mon. Not. R. Astron. Soc., 267, 1035
[44] Thompson C., 1994, Mon Not R Astron Soc, 270, 480
[45] Lyutikov M. and Blandford R., 2003 (astro-ph/0312347)
[46] Giannios D., Astron Astrophys. 2007, submitted (arXiv:0711.2632)
[47] Fan Y. Z., Zhang B., and Proga D., Astrophys. J., 2005, 635: L129
[48] Giannios D., Astron. Astrophys., 2006, 455: L5
[49] Fan Y. Z., Wei D. M., and Zhang B., Mon. Not. R. Astron. Soc., 2004, 354: 1031
[50] Blandford R. D. and McKee C. F., Phys. Fluids., 1976, 19: 1130
[51] Paczynski B. and Rhoads J. E., Astrophys. J., 1993, 418: L5
[52] Vietri M., Astrophys. J., 1995, 453: 883
[53] Gallant Y. A. and Achterberg A., Mon. Not. R. Astron. Soc., 1999, 305: L6
[54] Gallant Y. A., Lecture Notes in Physics., 2002, 589: 24
[55] Dermer C. D. and Humi M., Astrophys. J., 2001, 556: 479
[56] Virtanen J. P. and Vainio R., Astrophys. J., 2005, 621: 313
[57] Waxman E., Phys. Rev. Lett., 1995, 75: 386
[58] Cheng K. S. and Wei D. M., Mon. Not. R. Astron. Soc., 1996, 283: L133
[59] Rybicki G. B. and Lightman A. P., Radiative Processes in Astrophysics (Wiley, New York. 1979)
[60] Sari R., Piran T., and Narayan R., Astrophys. J., 1998, 497: L17
[61] Wijers R. A. M. J. and Galama T. J. Astrophys. J., 1999, 523: 177
[62] Totani T., Astrophys. J., 1998, 502: L13
[63] Zhang B. and Mészáros P., Astrophys. J., 2001, 559: 110
[64] Fan Y. Z., Zhang B., and Wei D. M., Astrophys. J., 2005, 629: 334
[65] Blumenthal G. R., Gould R. J., Rev. Mod. Phys., 1970, 42: 237
[66] Jones F. C., Phys. Rev., 1968, 167: 1159
[67] Sari R., Narayan R., and Piran T., Astrophys. J., 1996, 473: 204
[68] Sari R. and Esin A. A., Astrophys. J., 2001, 548: 787
[69] Stern B. E. and Poutanen J., Mon. Not. R. Astron. Soc., 2004, 352: L35
[70] Kobayashi S., Zhang B., Mészáros P., and Burrows D. N. Astrophys. J., 2007, 655: 391
[71] Aharonian F. A., Atoyan A. M., Astrophys. Spac. Sci., 1981, 79: 321
[72] Brunetti G., Astropart. Phys., 2000, 13: 107
[73] Plaga R., Nature., 1995, 374: 430
[74] Dai Z. G. and Lu T., Astrophys. J., 2002, 580: 1013
[75] Dai Z. G., Zhang B., Gou L. J., Mészáros P., and Waxman E., Astrophys. J., 2002, 580: L7
[76] Fan Y. Z., Dai Z. G., and Wei D. M., Astron. Astrophys., 2004, 415: 483
[77] Murase K., Asano K., and Nagataki S., Astrophys. J., 2007, 671: 1886
[78] Ichiki K., Inoue S., and Takahashi K., Astrophys. J., 2007, in press (arXiv:astroph/0711.1589)
[79] Dermer C. D., 2007 (arXiv:0711.2804)
[80] Piran T., 2003, Nature, 422: 268
[81] Shemi A. and Piran T., Astrophys. J., 1990, 365: L55
[82] Lithwick Y. and Sari R., Astrophys. J., 2001, 555: 540
[83] Molinari E., et al., Astron. Astrophys., 2007, 469: L13
[84] Narayan R., Paczyński B., and Piran T., Astrophys. J., 1992, 395: L83
[85] Paczynski B. and Xu G. H., Astrophys. J., 1994, 427: 708
[86] Rees M. J. and Mészáros P., Astrophys. J., 1994, 430: L93
[87] Kobayashi S., Piran T., and Sari R., Astrophys. J., 1997, 490: 92
[88] Sari R. and Piran T., Astrophys. J., 1995, 455: L143
[89] Sari R. and Piran T., Astrophys. J., 1999, 517: L109
[90] Akerlof C., et al., Nature, 1999, 398: 400
[91] Boër M., Atteia J. L., Damerdji Y., Gendre B., Klotz A., and Stratta G. Astrophys. J., 2006, 638: L71

[92] Rees M. J. and Mészáros P., Mon. Not. R. Astron. Soc., 1992, 258: 41
[93] Katz J. I., Astrophys. J., 1994, 423: L107
[94] Huang Y. F., Gou L. J., Dai Z. G., and Lu T., Astrophys. J., 2000, 543: 90
[95] Panaitescu A. and Kumar P., Astrophys. J., 2002, 571: 779
[96] Rhoads J. E., Astrophys. J., 1999, 525: 737
[97] Sari R, Piran T., and Halpern J. P., Astrophys. J., 1999, 519: L17
[98] Mészáros P, Rees M. J., and Wijers R. A. M. J., Astrophys. J., 1998, 499: 301
[99] Dai Z. G. and Lu T., Mon. Not. R. Astron. Soc., 1998, 298: 87
[100] Chevalier R. A. and Li Z. Y., Astrophys. J., 2000, 536: 195
[101] Paczyński B., Astrophys. J., 1998, 494: L45
[102] Rees M. J. and Mészáros P. Astrophys. J., 1998, 496: L1
[103] Dai Z. G. and Lu T., Astron. Astrophys., 1998, 333: L87
[104] Cohen E. and Piran T., Astrophys. J., 1999, 518: 346
[105] Zhang B. and Mészáros P., Astrophys. J., 2001, 552: L35
[106] Zhang B., et al., Astrophys. J., 2006, 642: 354
[107] Nousek J. A., et al., Astrophys. J., 2006, 642: 389
[108] Katz J. I., Piran T., and Sari R., Phys. Rev. Lett. 1998, 80: 1580
[109] Fan Y. Z., Piran T., and Xu D., J. Cos. Astropart. Phys., 2006, 0609: 013
[110] Fan Y. Z. and Wei D. M., Mon. Not. R. Astron. Soc., 2005, 364: L42
[111] Burrows D. N., et al., Science, 2005, 309: 1833
[112] Zou Y. C., Dai Z. G., and Xu D., Astrophys. J., 2006, 646: 1098
[113] Wu X. F., Dai Z. G., Wang X. Y., Huang Y. F., Feng L. L., and Lu T., Astrophys. J., 2005, submitted (astro-ph/0512555)
[114] Gao W. H. and Fan Y. Z., Chin. J. Astron. Astrophys., 2006, 6: 513
[115] Piro L., et al., Astrophys. J., 2005, 623: 314
[116] Chincarini G., et al., Astrophys. J., 2007, 671: 1903
[117] Troja E., et al., Astrophys. J., 2007, 665: 599
[118] Fan Y. Z. and Piran T., Mon. Not. R. Astron. Soc., 2006, 369: 197
[119] Panaitescu, A., et al., Mon. Not. R. Astron. Soc., 2006, 369: 2059
[120] Liang E. W., Zhang B. B., and Zhang B., Astrophys. J., 2007, 670: 565
[121] Mészáros P. and Rees M. J., Mon. Not. R. Astron. Soc., 1994, 269: L41
[122] Dermer C. D., Chiang J., and Mitman K. E., Astrophys. J., 2000, 537: 785
[123] Wang X. Y., Dai Z. G., and Lu T., Astrophys. J., 2001, 556: 1010
[124] Beloborodov A. M., Astrophys. J., 2005, 618: L13
[125] Wang X. Y., Li Z., and Mészáros P., Astrophys. J., 2006, 641: L89
[126] Pilla R. P. and Loeb A., Astrophys. J., 1998, 494: L167
[127] Fan Y. Z. and Wei D. M., Mon. Not. R. Astron. Soc., 2004, 351: 292
[128] Guetta D. and Granot J., Astrophys. J., 2003, 585: 885
[129] Wei D. M., Yan T., and Fan Y. Z., Astrophys. J., 2006, 636: L69
[130] Galli A. and Piro L., Astron. Astrophys., 2007, 475: 421
[131] Galli A. and Guetta D., Astron. Astrophys., 2008, 480: 5
[132] Fan Y. Z., Piran T., and Wei D. M., AIP Conf. Proc., 2008, 968: 32
[133] Nakar E., Piran T., Mon. Not. R. Astron. Soc., 2004, 353: 647
[134] Wang X. Y., Dai Z. G., and Lu T., Astrophys. J., 2001, 546: L33
[135] Granot J. and Guetta D., Astrophys. J., 2003, 598: L11
[136] Pe'er A. and Waxman E., Astrophys. J., 2004, 603: L1
[137] Piran T., Nakar E. and Granot J., AIP Conf. Proc., 2004, 727: 181
[138] Sari R. and Piran T., Astrophys. J., 1999, 520: 641
[139] Wang X. Y. and Mészáros P., Astrophys. J., 2006, 643: L95
[140] Klotz A., Gendre B., Stratta G., Atteira J. L.,Boer M., Malacrino F., Damerdji Y., and Behrend R., Astron. Astrophys., 2006, 451: L39
[141] Fan Y. Z., Dai Z. G., Huang Y. F., and Lu T., Chin. J. Astron. Astrophys., 2002, 2: 449
[142] Zhang B., Kobayashi S., and Mészáros P., Astrophys. J., 2003, 595: 950
[143] Kumar P. and Panaitescu A., Mon. Not. R. Astron. Soc., 2003, 346: 905
[144] Nakar E. and Piran T., Astrophys. J., 2005, 619: L147
[145] Shao L. and Dai Z. G., Astrophys. J., 2005, 633: 1027
[146] McMahon E., Kumar P. and Piran T., 2006, Mon. Not. R. Astron. Soc., 366: 575
[147] Wei D. M. and Fan Y. Z., Chin. J. Astron. Astrophys., 2007, 7: 509
[148] Ioka K., Toma K., Yamazaki R., and Nakamura T., Astron. Astrophys., 2006, 458: 7
[149] Mao J. R. and Wang J. C., Astrophys. J., 2008, submitted (arXiv:0801.0855)
[150] Gou L. J. and Mészáros P., Astrophys. J., 2007, 668: 392
[151] Yu Y. W., Liu X. W., and Dai Z. G., Astrophys. J., 2007, 671: 637
[152] Fan Y. Z. and Piran T., Mon. Not. R. Astron. Soc., 2006, 370: L24
[153] Shemi A., 1994, Mon. Not. R. Astron. Soc. 269: 1112
[154] Shaviv N. J. and Dar A., Astrophys. J., 1995, 447: 863
[155] Shaviv N. J. and Dar A., Mon. Not. R. Astron. Soc., 1995, 277: 287
[156] Lazzati D., Rossi E., Ghisellini G., and Rees M. J., Mon. Not. R. Astron. Soc., 2004, 347: L1
[157] Takagi R. and Kobayashi S., Astrophys. J., 2005, 622: L25
[158] Panaitescu A., Mon. Not. R. Astron. Soc., 2008, 383: 1143
[159] Panaitescu A., Mon. Not. R. Astron. Soc., 2008, 385: 1628
[160] Katz J. I., Astrophys. J., 1994, 432: L27
[161] Derishev E. V., Kocharovsky V. V., and Kocharovsky V. Vl., Astrophys. J., 1999, 521: 640
[162] Bahcall J. N. and Mśzáros P., Phys. Rev. Lett., 2000, 85: 1362
[163] Razzaque S. and Mśzáros P., Astrophys. J., 2006, 650: 998
[164] Dermer C. D. and Atoyan A., Astron. Astrophys., 2004, 418: L5
[165] Ioka K., Kobayashi S., and Mészáros P., Astrophys. J., 2004, 613: L17

[166] Cheng L. X. and Cheng K. S., Astrophys. J., 1996, 459: L79
[167] Wang X. Y., Cheng K. S., Dai Z. G., and Lu T., Astrophys. J., 2004, 604: 306
[168] Razzaque S., Mészáros P., and Zhang B., Astrophys. J., 2004, 613: 1072
[169] Zou Y. C. et al., Mon. Not. R. Astron. Soc., 2008, to be submitted
[170] Racusin J. L., et al., Nature, 2008 (arXiv:0805.1557)
[171] Xue R. R., Tam P. H., Wagner S. J., Behera B., Fan Y. Z., and Wei D. M., Astrophys. J., 2008, to be submitted
[172] Gupta N. and Zhang B., Mon. Not. R. Astron. Soc., 2008, 384: L11